LUND UNIVERSITY

Towards high efficiency nanowire solar cells

Otnes, Gaute; Borgström, Magnus T.

Towards high efficiency nanowire solar cells

Gaute Otnes and Magnus T. Borgström

Division of Solid State Physics and NanoLund, Lund University, P.O. Box 118, SE-221 00 Lund, Sweden

GRAPHICAL ABSTRACT
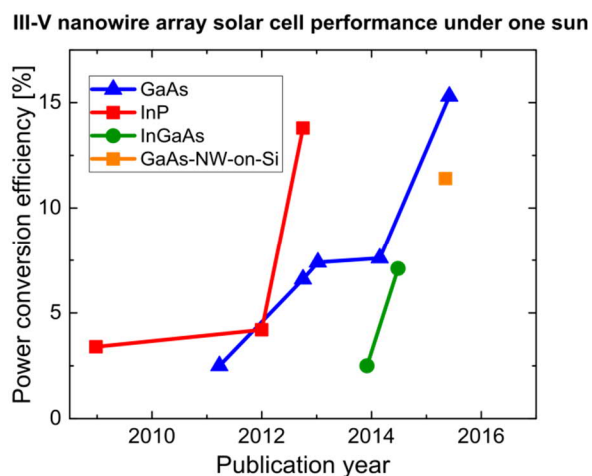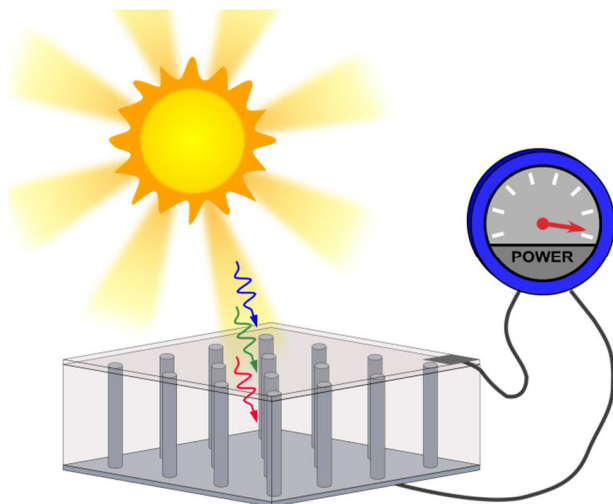
SUMMARY Semiconductor nanowires are a class of materials recently gaining increasing interest for solar cell applications. In this article we review the development of the field with a special focus on the III-V materials due to their potential to reach high power conversion efficiencies. After introducing basic concepts of nanowire synthesis, we discuss important aspects of nanowire design for high power conversion efficiencies; first in terms of light absorption, then in terms of charge carrier separation and collection. Further, we examine methods to assess and understand the materials quality and the solar cell performance. We end the review by a discussion of strategies and challenges in achieving efficiencies above the Shockley-Queisser limit, and the potential for cost efficient production.

KEYWORDS Nanowire; Solar cell; Semiconductors; Efficiencies

Introduction

One of the greatest challenges to mankind in the 21st century is the transition from an energy system based on fossil fuels to one based on sustainable and renewable resources [1], in which solar cells converting sunlight directly into electricity will play a central role. Installed capacity for solar energy production has increased exponentially since the beginning of the century, experiencing an average annual growth rate of about 40 % [2], driven by a rapidly decreasing cost and strong political subsidies. To maintain high growth in installed capacity and make solar energy a major contributor in the energy mix, increasing the solar cell power conversion efficiency (*PCE*) is especially important since it will cut all costs scaling with system size, and therefore have a much larger impact on total system cost than an equivalent decrease in cell production cost [3,4]. While close to the entire terrestrial solar cell market today is based on planar single junction solar cells, limited in *PCE* by the Shockley-Queisser limit of about 33 %, a wide number of concepts are actively pursued to reach higher *PCE* [5–8]. Amongst these, an increasing effort has in recent years been devoted to the use of nanostructured solar cell materials [9,10].

Semiconductor nanowires are high aspect ratio structures where two dimensions have length scales between a few and hundreds of nanometers, which have found promising applications in a wide range of areas [11]. Due to the small dimensions of the nanowires, they have several characteristics making them interesting for solar cell applications [12–14]. nanowire solar cells have developed rapidly over the last decade, increasing their *PCE* from the 5 % range to above 15 % in the last 5 years. In this paper we will review the knowledge obtained from the research on achieving high efficiency nanowire solar cells, and discuss how *PCE* can be improved further, ultimately past the Shockley-Queisser limit, while reducing cost.

III-V materials have excellent electronic and optical properties, and by tuning alloy composition a variety of bandgaps with almost a perfect fit to the solar spectrum can be synthesized. Solar cells made from III-V materials present the highest reported *PCE* for both single- and multi- junction planar [15] as well as for nanowire solar cell devices [16,17]. Therefore, the III-V materials system will be our main focus in this review. Note however, that several other materials in the nanowire geometry have been studied for solar

2

energy harvesting; most extensively Si [18–26], but also others such as CdS/CuS$_2$ [27], CdS/CdTe [28], perovskites [29] and III-N [30–32]. We will strive to include important results from these materials systems when appropriate.

We start by introducing important aspects for nanowire synthesis; basics of nanowire growth and the importance of the growth substrate and its patterning process. Thereafter, we discuss key guidelines obtained from experiments and modelling in how a nanowire array solar cell should be designed; first to maximize sunlight absorption, and second to achieve efficient charge carrier separation and extraction. Further, we review methods to assess and understand the nanowire solar cell performance. Finally, we conclude with a discussion of possibilities to reduce cost and to reach efficiencies beyond the Shockley-Queisser limit for nanowire based solar cells.

Nanowire synthesis

A range of methods exists to fabricate III-V nanowires, both top-down and bottom-up approaches. Many of the benefits of III-V nanowires as a solar cell material, such as materials savings and freedom in material design, are largely lost when using a top-down fabrication approach. In this review we will therefore focus on bottom-up nanowire synthesis, more specifically gas-phase epitaxial free-standing nanowire growth. This class of synthesis techniques has been heavily studied for more than a decade, and a high level of control is established when it comes to nanowire geometry, crystal structure, doping, and heterostructure formation. So far, III-V nanowires for solar cell applications have mainly been grown by metal-organic vapor phase epitaxy (MOVPE) and molecular beam epitaxy (MBE). Other gas-phase epitaxy techniques such as chemical beam epitaxy [33], laser ablation [34] and hydride vapor phase epitaxy [35] have also been used for nanowire growth. In-depth reviews of the nanowire growth mechanism are available [11,36–38] (other bottom-up synthesis methods are discussed in refs. [11,38]), and we will here briefly introduce the main aspects of nanowire synthesis relevant to the discussions in this topical review.

The most common and well-studied approach for nanowire synthesis is to use a metal seed particle to mediate growth through the vapor-liquid-solid (VLS) mechanism [39]. The constituent atoms of the growing crystal, including any dopants, are provided in the vapor phase. For III-V materials, at least one of these growth species, typically the group III element, is dissolved in the seed particle. While a high level of synthesis control has been established, the exact growth mechanism, for instance the detailed incorporation pathways of the group V element, is still under debate. The seed particle is most often in a liquid state during synthesis, even though growth from a solid particle in a vapor-solid-solid mechanism [40,41] is also possible. While supersaturation in the vapor and liquid phase create the thermodynamic force driving the growth species towards incorporation in the solid crystal, kinetically limited growth conditions lets preferential interface nucleation at the liquid-solid interface ensure growth predominantly in one direction [37]. To provide such growth conditions, most nanowires are grown at relatively low temperatures (350-550 °C). So far, a metal seed particle of an element foreign to the growing material has been most commonly used, with gold being the predominant material of choice. Other foreign metals for nanowire synthesis have been studied [42] and might prove useful for nanowire solar cell fabrication in the future, but will not be discussed further here. It is also possible to use a metal particle native to the grown semiconductor, such as Ga in the growth of GaAs [43], in what is commonly referred to as self-catalyzed or self-seeded growth.

As an alternative to the metal-catalyzed growth mechanism for nanowires, selective area growth has attracted increasing attention in recent years, mainly pioneered by the Fukui group [44,45]. Using this technique for nanowire synthesis, holes in an inert mask on the growth substrate facilitate nucleation only in certain locations. When growth conditions are carefully tailored, low-index faceted nanowires are formed at these locations, and the difference in nucleation energy on the different facets ensures continued one-dimensional growth [46]. The selective area growth is typically carried out at higher temperatures (500-750 °C) than VLS-growth.

Nanowire heterostructures

An important benefit in nanowire growth is the possibility to create heterostructures with reduced requirements on lattice matching. For axial heterostructures (Fig. 1a), created by changing growth precursors during axial nanowire growth, efficient strain relaxation via the free surface enables high quality heterostructure materials unavailable in planar growth [47–51]. Radial nanowire heterostructures (Fig. 1b) can be grown by altering growth conditions during synthesis from promotion of axial to promotion of radial growth. This was first realized by Lauhon et al. [52], in the Si-Ge system. The shell is grown by deposition through the vapor-solid mechanism similar to layer growth, with the nanowire side facets acting as the growth substrate. Most often, this means growth at higher temperature for the shell compared to the core. Note that, above a certain diameter of the nanowire core, lattice matching requirements will become limiting for the shell growth. Reviews of growth and applications of nanowire based axial and radial heterostructures are given in refs. [53,54]. For nanowire solar cells, these approaches can be used for example to create surface passivating shells and tandem nanowire solar cell structures, as will be discussed later.
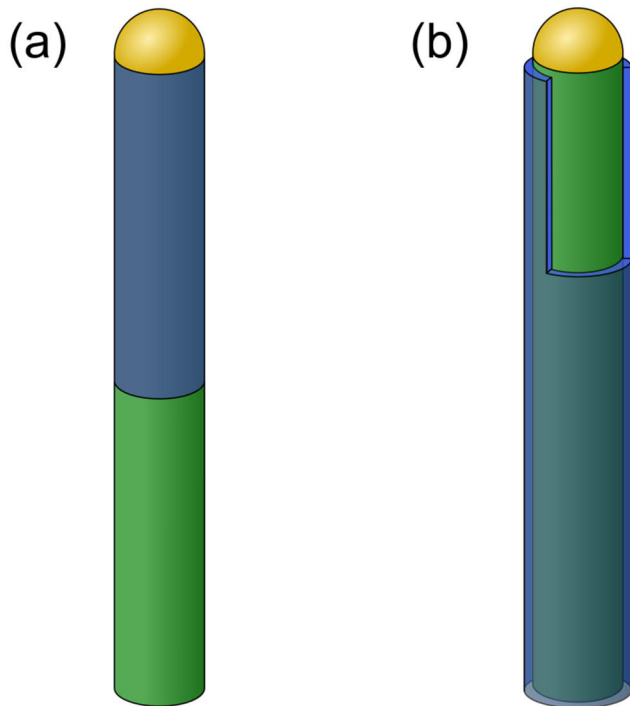
Figure 1 **Schematic of nanowire heterostructures.** Nanowire heterostructures can be created in both the axial (a) and radial (b) direction, by changing growth conditions during synthesis. In (b), a part of the shell is removed to reveal the core. Green and blue colors indicate different materials. The sketch can also illustrate axial and radial *p-n* junctions, with the green and blue parts indicating different type of doping.

Growth substrates

The growth substrate is a key element in any epitaxial growth process, both in terms of materials quality and cost. As thoroughly reviewed in ref. [55] III-V nanowires can grow in a range of different crystal directions, but normally growth proceeds along the low-energy (111) (or, for wurtzite: (0001)) direction. The vast majority of studies on III-V nanowire solar cells therefore utilize growth from native (111) substrates, resulting in nanowire arrays standing vertically with respect to the substrate surface.

In planar III-V photovoltaic (PV) technology, lattice matching requirements severely limit the number of possible substrates for growth, and high-cost substrates such as Ge are usually employed [56]. In the nanowire geometry, the aforementioned relaxed lattice-matching requirements enable heteroepitaxy of III-V nanowires on a wide range of substrates, potentially much cheaper and better suited for large scale processing. Amongst the foreign substrates, nanowire growth on Si [57–60] has attracted most attention for solar cell applications due to the possibility to create nanowire-on-planar-Si tandem junctions, which will be further discussed towards the end of this review. III-V nanowire growth on other foreign substrates such as SiO_x/glass [48,61–63] or graphene/graphite [64–67] have been demonstrated, but is so far less developed.

Substrate patterning

For optimal performance of a nanowire array solar cell, growth from patterned substrates is a key requirement. Even though optical absorption might not be limited by inhomogeneity in the nanowire array

[68], it is of importance to optimize all nanowires uniformly in terms of key parameters such as doping profiles, passivation layers and emitter lengths. A patterned substrate functions as a template for nanowire array growth, and the equidistant spacing and equal size of the growth centers ensures that all nanowires experience similar growth conditions. Depending on the growth mode, the pattern consists of holes in a growth mask for selective area and self-catalyzed growth, while gold particles with or without a surrounding growth mask can be used for gold-catalyzed growth.

Several lithographic techniques have been employed for pattern formation for nanowire growth, as reviewed by Fan et al [69]. Electron beam lithography (EBL) has been used extensively for growth of nanowires in a controlled array [70–74] and offers great flexibility in pattern design, but is employing slow sequential pattern writing. In comparison, nanoimprint lithography (NIL) has emerged as a promising candidate for high-throughput and low-cost patterning for nanowire array growth [75–79], offering full wafer processing and industrial compatibility [80]. Other techniques with potential benefits have been utilized for nanowire growth, such as deep-UV lithography [81], laser interference lithography [82,83], nanosphere lithography [68,84] and block copolymer lithography [85].

We note that even after the pattern on the substrate is successfully produced it might require significant optimization to preserve the pattern through the stages of nanowire growth, due to problems such as seed particle displacement [79] and surface contamination from the patterning procedure [76]. Considering the complex interplay between seed particle pattern formation and nanowire growth conditions, we believe that an untapped potential exists in extended collaborations between experts in the different fields of nanopatterning and nanowire synthesis.

Nanowire design for optimal sunlight absorption

The first step in converting solar energy into electricity is the absorption of sunlight. One of the most exciting features of nanowires as a solar cell material is the geometry dependent absorption characteristics [86–91], giving them light interaction features not found in a bulk material. While a lot of

important work has been devoted to absorption in horizontal nanowires, we will in the following focus on vertically oriented nanowire arrays, in our opinion the most promising configuration for large area solar energy harvesting by nanowires.

Tuning geometrically dependent absorption resonances in nanowire arrays

It is well established that an array of subwavelength diameter nanowires can absorb more light than a thin-film made of the same amount of material [92–96], and that wave-optics instead of ray-optics is needed to give a proper description of these systems [16]. Importantly, vertical nanowires have been shown to absorb light from a larger area than their physical cross-section [97]. The geometry of a vertical nanowire array is set by four different parameters (Fig. 2a); nanowire diameter, nanowire length, array pitch, and array symmetry. We note that extensive important work has been done on understanding absorption in Si nanowire arrays, with a selection given as refs. [92,98–104]. However, due to the substantially different absorption characteristics of direct and indirect bandgap materials, care should be taken if transferring knowledge directly between Si and III-V materials. We will base our discussion of optimizing absorption mainly on studies published on direct bandgap nanowires, relevant to the III-V materials which at low material use offer efficient light absorption, also close to the bandgap.

The optical modes in nanowire arrays are strongly dependent on nanowire diameter, but less dependent on the array pitch and nanowire length [96,105–107]. This indicates that the modes are inherent to the single nanowire, and several authors report that they do in fact originate from the HE_{1n} waveguide modes in individual nanowires [93,107,108]. Anttu and Xu [107] found a maximized ultimate efficiency [109] for an InP nanowire array solar cell when the absorption resonance energy was placed close to the bandgap of the material, where the absorption coefficient is smaller than at higher energies, and proposed this resonant absorption enhancement to be a general design rule. Its validity is supported by other studies on both InP [93,96,110] and GaAs [94,96,108,111–113] where an optimized sunlight absorption efficiency

is found at nanowire diameters of 150-180 nm, where light with energy close to the bandgap is efficiently coupled into the HE_{11} waveguide mode for InP and GaAs nanowires (for InP, see Fig. 2b). Furthermore, Anttu and Xu outlined a simple rescaling method to obtain these optimal diameters for other direct bandgap semiconductors, based on their bandgap and refractive index [107].
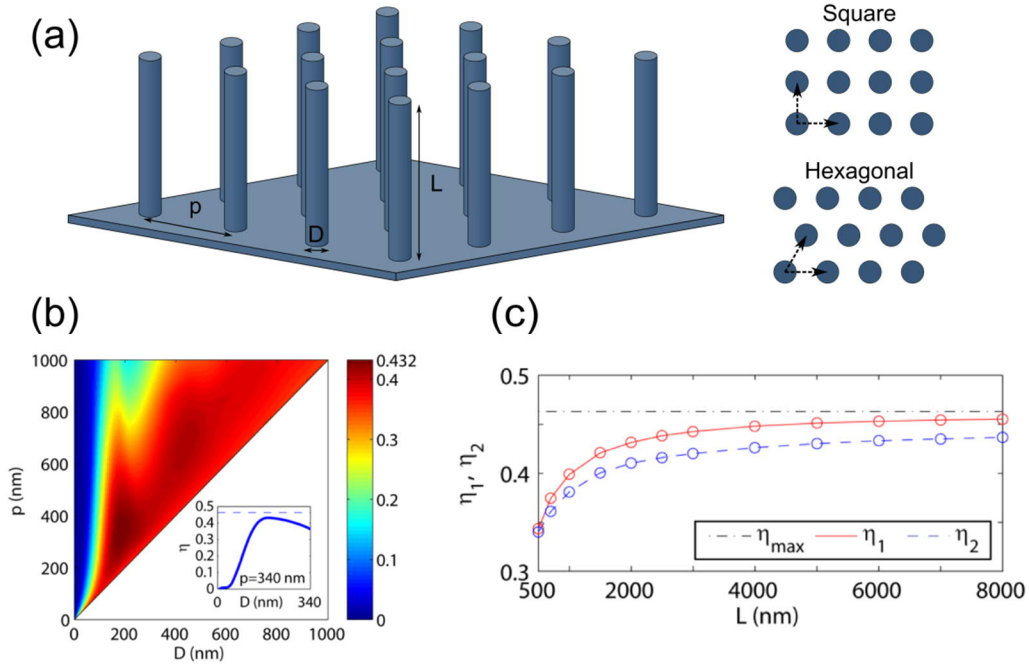
Figure 2 **Geometry dependence of absorption in a nanowire array.** (a) Sketch illustrating the four parameters defining the geometry of a nanowire array; nanowire length (*L*), nanowire diameter (*D*), array pitch (*p*) and array symmetry (exemplified by the two most common: square and hexagonal). (b) Ultimate efficiency (η) of an InP nanowire array as a function of *p* and *D* for a fixed *L* = 2000 nm. Two local maxima can be seen, η_1 and η_2. The inset shows a line-cut of η as a function of *D* for *p* = 340 nm (solid line). In this inset is shown also η_{max} = 0.463 (dashed line), the maximum possible ultimate efficiency of InP. (c) Maximum ultimate efficiency for η_1 (solid red line) and η_2 (dashed blue line) plotted against *L*. η_{max} is also shown (dashed-dotted black line). (b) and (c) reprinted from [107]. Copyright 2013 OSA.

If going to bigger diameters than the optimal, the resonance energy moves into the non-absorbing regime of the semiconductor [108]. Higher order modes such as the HE_{12} can then be used instead, at the expense of somewhat weaker coupling [108,111]. In addition, with increased diameters, issues with lattice matching requirements become more relevant. At much smaller nanowire diameters than the optimal, absorption at long wavelengths is lost [93,107,114], which cannot be compensated by denser packing of the array.

Importantly, the nanowire array can act as an antireflection (AR) layer. For example, the reflection from thin nanowires is much lower than for a thin film due to an enhanced transmission [95,105]. This can be understood as the nanowires providing an effective refractive index between that of air and the underlying substrate, suppressing reflection across a wide range of wavelengths [115,116]. This effect is also present in thicker nanowires, and in nanowire-on-planar tandem solar cell designs where the nanowires can act both as a top-cell absorbing light above its bandgap, and as an AR coating for the non-absorbed wavelengths transmitted to the bottom cell [114]. By allowing for dual-diameter or graded diameters, the nanowire geometry can be used fully to optimize light absorption [117,118].

With nanowire diameter tuned to optimize the sunlight absorption of the individual nanowires, efficiencies can be further improved by changing the other geometrical parameters to maximize the amount of absorbing semiconductor material in the array while keeping the insertion reflection losses at the top surface low [107]. For instance, an increasing nanowire length benefits absorption until approaching a saturation limit [96,106,119] (Fig. 2c), while for a fixed length and diameter an optimum in pitch is generally found [68,93,106,107] (Fig. 2b). The final geometrical parameter of array symmetry has in comparison to the others been found to have little effect on the absorption properties [120]. We note that to optimize carrier extraction and/or ease growth and fabrication requirements in actual devices, some compromises might be needed with regard to the length and pitch giving the maximum absorption.

The discussion above regarding optimal geometries for light absorption is largely based on theoretical work, but experimental studies also confirm the outlined trends and have proven the strong absorption possible in nanowire arrays [108,119,121]. To optimize light absorption, the processing of the nanowire array into full solar cells introduces additional parameters that might be tuned. For instance, it has been shown that a dielectric shell can have a significant influence on nanowire light absorption [122–124], while the shape of the ITO top contact can be used to improve light coupling into the nanowire array [125]. For use without a solar tracking unit, an important point is that the nanowire array solar cells maintain their excellent absorption and AR characteristics up to incidence angles as high as 60 ° [116,126,127].

Nanowire design for optimal charge carrier separation and collection

Once free electrons and holes have been generated by the absorption of light, they need to be separated and collected through an external circuit. The efficiency of this process will be determined by the electronic properties of the device. In the following we will discuss central concepts affecting the electronic properties of nanowire array solar cells: crystal structure, doping control, junction geometry and design, surface passivation and cleaning, and contact formation.

Crystal structure can affect charge carrier transport

While in bulk all III-V semiconductors except the nitrides form in the zincblende (ZB) crystal structure, in nanowires they can form in both ZB and wurtzite (WZ), but most commonly in a mixture of the two, as was observed already in the pioneering work in the 90s by the Hiruma group [128,129]. What drives the formation of the different phases has been an area of intense study, and it has been shown to strongly depend on growth conditions such as temperature [130,131], impurity doping [132,133] and V-III ratio [134–137]. From a theoretical perspective, the effect of several parameters on the nucleation of different phases has been modelled [138–140], such as supersaturation (growth rate), particle size and

differences in interface energy between solid-liquid, solid-vapor and liquid-vapor. An environmental transmission electron microscope was recently used to study the growth of a GaAs nanowire, where the seed particle geometry was observed to determine the formation of different crystal phases [141].

The nanowire crystal structure has been shown to affect electrical transport [142–149]. For instance, in InP nanowires of predominantly WZ crystal phase, ZB segments can act to scatter [146] and trap carriers [145], dominating the electrical transport characteristics also at room temperature. In InAs nanowires, Thelander et al. [144] showed that while single planar defects (twin planes in ZB, stacking faults in WZ) had little effect on the resistivity, longer segments of alternating ZB and WZ crystal structures did. Together with the recent advances in understanding the crystal phase formation in III-V nanowires, high phase purity nanowires have been achieved by several growth mechanisms [150–152] and in different materials [153–157]. However, for a solar cell device, growth conditions cannot be optimized for crystal structure alone, but factors such as efficient dopant incorporation, reduced vacancy formation, controlled non-intentional doping, and minimized tapering also need to be considered. This has made it difficult to experimentally establish how and when crystal structure effects will start limiting *PCE* in nanowire based solar cells, but it seems clear that achieving high and controlled crystal purity remains a challenge to produce III-V nanowire array solar cells with high *PCE*.

Nanowire doping control

Recall that nanowires are typically grown in the kinetically limited regime in the presence of a metal catalyst. Therefore, in situ nanowire dopant incorporation can be quite different from that in thin-film epitaxy, and the introduction of dopants can strongly affect the overall growth dynamics. A thorough review of nanowire doping is provided in [158], and we will here only highlight some important aspects and recent results.

To optimize a nanowire solar cell device towards high efficiencies by guidance of predictions from modelling, experimental quantitative information about actual doping levels is needed. Since growth conditions and thereby dopant incorporation can change both axially and radially during growth, it is important to be able to obtain spatially resolved information on carrier concentrations. Such information can be obtained from Hall-effect measurements, which is the standard technique to obtain doping information in bulk semiconductors. Hall measurements on nanowires are challenging due to the small dimensions and complex geometry, and was only shown as late as 2012 [159,160]. Lately, systematic studies have been performed using Hall effect measurements as a benchmark to quantitatively validate other commonly deployed techniques such as photoluminescence (PL) [161] and field effect measurements [162]. Evaluating nanowire doping by PL [163,164] and other optical techniques such as transient terahertz photoconductivity [142] and Raman spectroscopy [165,166] are important since they can be applied in a contactless manner, and hence provide rapid feedback for growth development. For extremely high resolution characterization, which might be needed to properly evaluate and troubleshoot e.g. nanowire tunnel junctions, atom probe tomography could prove to be a powerful technique [167,168].

We note that while significant knowledge has been accumulated on doping of binary grown III-V nanowires, much less is known about the doping of the complex ternary materials needed for optimal bandgap tuning in tandem structures.

Junction geometries

Two main nanowire *p-n* junction geometries exist where a single-material nanowire constitutes the sole active region in the solar cell device, illustrated in Fig. 1. In the axial junction geometry (Fig. 1a), the doped layers are stacked on top of each other in the axial direction, analogous to a thin film solar cell. In the radial junction geometry (Fig. 1b), a doped core is surrounded by an oppositely doped shell. The *p-n* junction in each nanowire is normally created by changing dopant precursors during axial or radial growth, analogous

to the axial or radial nanowire heterostructures discussed previously. In the following we will highlight some differences and similarities between the two geometries.

Nanowires with both radial and axial junctions can be tailored to benefit from resonant light absorption, and can leverage relaxed lattice matching requirements to be grown on foreign low-cost substrates. However, while some tandem architectures have been suggested based on radial junctions [169–172], these appear experimentally challenging to realize. With a junction formed along the axial direction of the nanowire on the other hand, a tandem architecture is easily envisioned based on the extensive work done on nanowire heterostructures, as outlined earlier. The main benefit of the radial structure is instead the decoupling of the directions of light absorption and charge separation, as originally proposed by Kayes, Atwater and Lewis [173]. In a planar solar cell (or an axial junction nanowire solar cell) a certain film thickness (nanowire length) will be necessary to absorb a sufficient amount of the incoming light, but at the same time the emitter and the base must be kept thin enough to allow minority carriers to diffuse to the junction, setting a limit to the total thickness of the device. If the charge carriers instead are separated across a radial junction, the nanowire length can be kept long to allow for strong absorption, given that the minority carrier diffusion length is longer than approximately the nanowire radius. This will significantly decrease the vulnerability to bulk defects which decrease minority carrier lifetimes, and allow for high efficiencies with lower materials quality than in a planar device. However, as Kayes et al. highlighted [173], this effect will mainly be beneficial in indirect bandgap materials such as Si, where thick films/long nanowires will be needed for sufficient absorption. Note that two factors complicate experimental realization of the predicted performance benefits of the radial geometry. First, in their original work Kayes et al. pointed out that while the radial geometry is more tolerant to defects in the quasi-neutral regions of the device, the open circuit voltage (V_{OC}) of the cell will be strongly affected by the trap density in the depletion region [173]. Second, the radial geometry shows a strong sensitivity to doping levels, where high and balanced doping levels are needed to prevent full depletion of one side of the junction [111,113,174–176]. Thus, high quality radial junctions with controlled and uniform doping both in the core and shell are required. Comparing the best

experimental devices of the two geometries, we see that while radial devices [120,177] can reach short circuit current density (J_{SC}) comparable to the best axial ones [16,17], the best reported V_{OC} and fill factor (*FF*) values [125,178] are significantly lower for the radial case, leading to less than half the *PCE* of the best axial cells. Thus, any benefits of the radial structure in terms of charge carrier collection has until now been masked by other dominating factors.

The reasons for the seemingly low quality radial junctions are not immediately clear, but we will identify some possible contributing factors. First, one might argue that the vapor-solid compared to the vapor-liquid-solid mechanism could yield better quality growth. However the commonly mixed nanowire core crystal structure has been observed to strongly affect shell growth [179–181], making it a non-ideal growth substrate. Further, dopant incorporation is facet dependent [182–184], and the presence of dopants during synthesis have been observed to strongly affect shell growth dynamics and uniformity [185,186]; hence achieving homogeneous doping can be a challenge. Additionally, when heating the sample to higher temperatures to grow a shell in the mass flow limited growth regime, out-diffusion of dopants from the core might be an issue. Furthermore, for catalyzed nanowire growth, the nanowires are often removed from the growth chamber in order to remove the catalyst seed particle between core and shell growth, to facilitate predominant radial over axial growth. This removal from the growth chamber exposes the surface to oxidation, likely to deteriorate interface properties. The problems with high quality radial junction formation during epitaxial growth can potentially be avoided by using ex-situ molecular monolayer doping to form the junction, which has yielded a V_{OC} of 0.54 V in a top-down fabricated InP nanowire array solar cell [187], amongst the highest values reported for the radial geometry.

The attainable V_{OC} might be different between a planar solar cell and nanowire solar cells with radial or axial junctions, due to differences in junction area [16,174,188,189]. This can be understood by considering the equation $V_{OC} \approx (kT/q) \times \ln(I_{SC}/I_0)$, where k is the Boltzmann constant, T is temperature, q is the elementary charge, I_{SC} is the short-circuit current and I_0 is the saturation current. Due to the light concentration originating from the previously discussed resonant absorption, I_{SC} in the nanowire solar cells

could be as high as in a planar solar cell. However, assuming a cell limited by non-radiative recombination in the depletion region, we will have $I_0 = J_0 \times A_{junction}$, where J_0 is the saturation current density and $A_{junction}$ is the junction area. If so, and if assuming J_0 similar in the nanowire and the planar material, I_0 can be lower (higher) in an axial (radial) nanowire junction than in a planar one due to the smaller (larger) $A_{junction}$, thus potentially giving a higher (lower) V_{OC} in the axial (radial) nanowire solar cell.

For the synthesis of the axial junction, suppressing unintended radial growth is a key to prevent electrical shorting of the junction [190]. In situ etching during gold-catalyzed nanowire growth has proven to be a powerful tool to take complete control of axial versus radial growth, successfully used in nanowires of several III-V materials relevant to solar energy harvesting [191–193]. It should be pointed out that the axial geometry is considered more susceptible to high surface recombination, and also requires more precision in top contact formation. These challenges will be discussed in later sections.

A range of other approaches exists where the nanowire is only one of the parts forming the charge separating junction, such as nanowire-embedded-in-thin-film heterojunctions [28], nanowire-substrate heterojunctions [30,194], nanowire-ITO heterojunctions [195], nanowire-metal Schottky solar cells [196,197], nanowire-polymer hybrid devices [198–202], nanowire-dye sensitized cells [203–205] and nanowire-electrolyte photoelectrochemical cells [206,207]. While aspects covered here are relevant also to many of these architectures, a detailed discussion of the specifics of each is beyond the scope of this review.

p-n junction segment lengths and doping levels

The optimal design of the nanowire *p-n* junction for charge carrier extraction will vary depending on exact geometry, surface passivation etc. However, some general guidelines have been established. In the following we will adhere to the common solar cell terminology of emitter and base for the top/shell and bottom/core parts of the axial/radial *p-n* junctions.

In fabricated axial nanowire array solar cells it has been found that a large portion of the photogenerated carriers are lost in the emitter [16,111]. This can be understood by considering that the biggest portion of the light, especially for short wavelengths, will be absorbed at the top of the nanowires (Fig. 3a), thus in or close to the emitter. In the emitter however, most generated carriers will be lost due to recombination at the contact and due to minority carriers rapidly recombining with the large excess of majority carriers from the doping (the emitter is typically highly doped to ensure an Ohmic contact). Some strategies have been explored to avoid this problem. Wallentin et al. observed that reducing the nominal emitter length in an InP nanowire array solar cell from 360 nm to 60 nm increased J_{SC} by a factor of two, in good agreement with modelling when assuming that all carriers generated in the emitter are lost (Fig. 3b-d) [16]. Similar performance improvement was later achieved by reducing the emitter length in GaAs [111]. A highly doped minority carrier reflection barrier close to the contact could be introduced [111,208], which requires high precision in top contact formation and doping control during growth. Chen et al. [209] introduced the idea of growing an indirect bandgap material as an emitter layer, preventing absorption in the region of poor carrier collection.
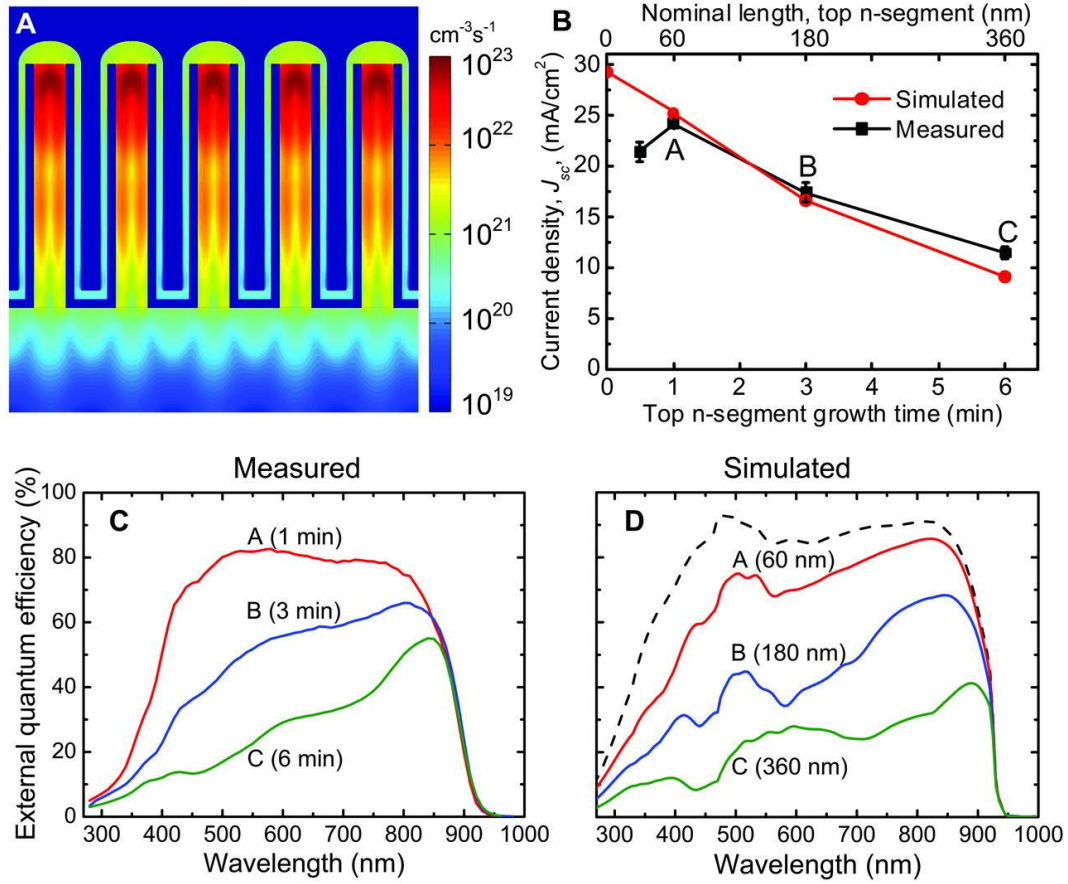
Figure 3 **InP nanowire solar cell with axial *p-n* junction; performance dependence on top n-segment length.** (a) Simulated optical generation rate of electron-hole pairs in the y-z cross section of an InP nanowire solar cell, for x polarized light. (b) Measured and simulated J_{SC} versus n-segment growth time. The error bars are one standard deviation. (c) Measured external quantum efficiency (*EQE*) of samples with n-segment growth time; 1 (A, red), 3 (B, blue) and 6 (C, green) minutes. (d) Simulated *EQE* of samples with different n-segment lengths; 60 (A, red), 180 (B, blue) and 360 (C, green) nanometers. Shown is also *EQE* for a sample with 60 nm n-segment, without losses (dashed line). From [16]. Reprinted with permission from AAAS.

Similarly to a short highly doped emitter, modelling indicate that a short highly doped back surface field (BSF) is beneficial [17]. In fact, results from the two highest performing nanowire solar cell devices

to date [16,17] indicate that for the axial geometry, an optimal design is where the main part of the nanowire is left nominally intrinsic or lowly doped, and with short highly doped emitter and BSF end segments. The nominally intrinsic/low-doped region serves as a long and efficient absorber area where electrons and holes are split by the built in electric field over the segment, while the highly doped ends ensure a high V_{OC} and prevents minority carriers from recombining at the contacts. Further, the inclusion of the nominally intrinsic segment might reduce the *p-n* junction interfacial recombination, as seen in single Si nanowire PV devices [20]. These design guidelines were lately supported by modelling by Trojnar et al. [210,211].

For the radial geometry perhaps the most important issue is to prevent complete carrier depletion of either of the segments, as discussed earlier. For this, high doping is needed, as well as a careful tuning of segment thicknesses to the exact doping levels [111,113,174,175]. As in the axial geometry, a highly doped emitter can be used for electrically transparent contact formation and the axial thickness of the emitter should be thin to avoid carrier loss [113,212]. Also in the radial geometry, the inclusion of a nominally intrinsic segment between the *p* and *n* doped part has been shown beneficial for the electrical properties [19,125,213].

Considering the importance of accurate control of nanowire segment lengths, optical reflectometry was recently shown as a powerful tool, able to monitor nanowire length and diameter in situ with high precision, on par to that of scanning electron microscopy [214].

Surface passivation and cleaning

Due to their large surface-to-volume-ratio, the electrical performance of nanowires can be strongly influenced by surface states. A poor surface with a high surface recombination velocity (*SRV*) can be detrimental for nanowire solar cell performance [111,114,174,212,215–217]. Of the two junction geometries, the axial is found to be more susceptible than the radial to high values of *SRV* [215,216]. However, with a *SRV* of ~10^3 cm/s or lower, it is generally found that surface recombination plays a small

role for the nanowire solar cell performance [212,215–217]. Different strategies have been developed to obtain appreciably good surface properties, which will be discussed in the following.

First it is important to note that significant differences exist in the surface properties of different III-V materials. InP is well-known to show low values of *SRV* [218,219], and a *SRV* as low as 170 cm/s has been measured for undoped InP nanowires [146]. Indeed, in high performing InP nanowire solar cells, no passivation has been applied other than the SiO_x coating used to electrically isolate the junction [16,220]. A passivating effect of the SiO_x coating was indicated by an increase in the PL lifetime [220]. However, unintended radial growth, surface oxides and carbon contaminants might degrade the good surface properties of InP, which can be alleviated by in situ [191] and/or ex situ [220,221] etching. For epitaxial passivation of InP, a suitable high bandgap and lattice matched material is not available, but lattice mismatched AlInP has been used resulting in solar cell performance enhancement [177].

For GaAs on the other hand, the surface poses a much more severe limitation where un-passivated GaAs nanowires were found to have *SRV* of $\sim 10^5$ cm/s [222] and minority carrier lifetimes on the order of tens to a few hundred picoseconds [223–226], making them unsuitable for high performing solar cells. However, several materials are available to epitaxially passivate GaAs, and passivating shells of InGaP [227–229], AlGaAs [224,225,230–234] and AlInP [226,235] have all been shown to give substantial improvement of optical and electrical properties for GaAs nanowires. These benefits have been utilized in GaAs nanowire solar cell devices. For instance, Åberg et al. [17] saw a reduction in dark saturation current by a factor of 2000 by passivating with an AlGaAs shell, while Mariani et al. [120] saw an increase in *PCE* of more than a factor of 6 when passivating with an InGaP shell, corresponding to a greatly improved external quantum efficiency (*EQE*), especially for short wavelengths (Fig. 4). An InGaP shell also gave significant performance improvements in a GaAsP single nanowire PV device [236]. Thin layers of non-lattice matched materials such as GaP could also potentially be used [237], where the use of a binary material would reduce complexity in shell growth.
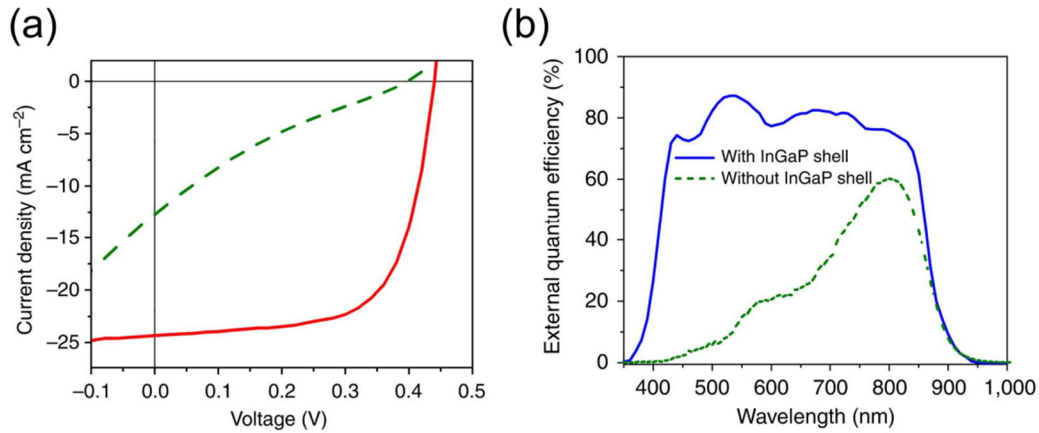
Figure 4 **Effect of in situ InGaP shell passivation on GaAs nanowire solar cell performance.** (a) Current density-voltage characteristics under air mass 1.5 global illumination conditions for solar cells with (solid red line) and without in situ InGaP shell (dashed green line) . InGaP- passivated solar cells show an open-circuit voltage of 0.44 V, short-circuit current density of 24.3 mA cm^{-2} and fill-factor of 62 %. This translates into a power conversion efficiency that amounts to 6.63 %. (b) External quantum efficiency of processed GaAs nanowire solar cells with (solid blue line) and without (dashed green line) passivation. Reprinted by permission from Macmillan Publishers Ltd: Nature communications, [120], copyright 2013.

Thin passivation layers of sulfides [228,238–240] or nitrides [241] can be applied ex-situ by wet-chemical techniques, but these passivation layers are known to suffer from stability issues, and removal of the nanowires from the growth chamber before passivation make them susceptible to oxidation.

To assess the effect of different passivation schemes, both optical methods such as PL [223,242] or THz [243] spectroscopy and electrical methods such as field effect mobility [224,228,235] are used.

Is there a need for gold free synthesis methods?

A commonly raised concern regarding the widely employed gold-catalyzed growth mechanism is the possibility of degraded nanowire electrical properties by Au impurities. This is largely based on

experiences with Si, where Au forms detrimental deep-level traps [244] and have been reported to incorporate into nanowires [245]. It has been indicated that Au might incorporate in III-V nanowires during axial [246,247] and radial growth [248], possibly degrading PL properties in GaAs nanowires [249]. However, later studies on gold-catalyzed growth have reported amongst the best PL lifetimes seen for GaAs nanowires (~1-2 ns) [17,224,234,242,243]. Further, for nanowire solar cell devices, the highest performances to date have been achieved by gold-catalyzed growth methods both for InP and GaAs [16,17]. However, since nanowires have still not shown optical or solar cell performance on par to their planar counterparts, it is too early to rule out that Au can introduce detrimental defect states, even though most results indicate otherwise. We note that if the nanowires are to be grown directly on a Si solar cell in a tandem architecture, gold-free synthesis methods such as self-catalyzed or selective area growth are needed.

Contact formation

After the charge carriers have been separated by the *p-n* junction, Ohmic front and back contacts with low contact resistance are essential for efficient charge carrier collection. Contacting nanostructures might involve significant challenges, as discussed extensively in a review by Leonard et al. [250]. Here we will discuss some aspects relevant to nanowire array solar cells.

For the front contact in a nanowire array solar cell it is beneficial to contact the top of the nanowires only. If the contact extends too far down the sidewall of the nanowires, one might have recombination and carrier depletion at the contact-semiconductor interface strongly affect the device [208,212], and for an axial geometry one might risk to short-circuit the *p-n* junction. To contact only the top of the nanowire, a polymer planarization layer is often employed [251]. The front contact is usually a transparent conductive oxide, with indium-tin-oxide (ITO) being the most common. Mariani et al. compared ITO to aluminum-zinc-oxide as a front contact to GaAs nanowire solar cells, and found ITO to have superior performance in their setup [238]. To reduce contact resistance, a thin layer of Ti [120,125,252,253] or In [176,254] between the nanowires and the ITO has been used. Another well-known strategy to reduce contact resistance is to

introduce a highly doped layer at the semiconductor-metal interface. As an example, Nakai et al. [253] used this approach to greatly reduce series resistance in an InGaAs nanowire solar cell device, with accompanying improvements in *FF* and V_{OC}. If the nanowires are grown gold-catalyzed, the gold particle, even though offering an in situ defined metallic contact, should be removed prior to front-contact deposition to reduce reflection of incoming light [106].

It should be noted that Ohmic contact formation is material and doping dependent. For example, due to the surface Fermi level pinning in InP, *p*-type InP nanowires are hard to contact as compared to *n*-type material [190]. Depending on the contacting scheme, this might put constraints on the polarity of the *p-n* junction.

For the back contact, it has most commonly been formed through the growth substrate, where the large surface area gives good contact performance. New and potentially more challenging contacting schemes will be needed when more cost-effective synthesis strategies are adopted. Such strategies will be discussed in more detail in later sections.

Assessment of nanowire solar cells

Both single nanowire and full nanowire array measurements are important to develop and assess performance of nanowire solar cells. Single nanowire measurements are especially valuable to evaluate electrical characteristics inherent to the nanowires. As mentioned previously, single nanowire measurements are used extensively to obtain information about nanowire doping as well as effects of surface passivation. Contacting single nanowires instead of nanowire arrays is often relatively fast, and the measurements can be easier to interpret with respect to some characteristics since they avoid ensemble averaging and effects from non-uniform contacts. If good Ohmic contacts are realized, IV-sweeps can reveal information about the nanowire junction quality, for instance when going from a *p-n* to a *p-i-n* junction [19]. Further, techniques such as electron beam induced current (EBIC) [17,229,240,255–259], cathodoluminescence (CL) [111,260,261] and scanning photocurrent microscopy (SPCM) [21,262–265] measurements can

provide insights into charge separation and collection properties. As an example, Gutsche and Niepelt et al. used EBIC on single GaAs nanowire *p-n* junctions to determine minority carrier diffusion lengths, estimate *SRV* values, study effects of surface passivation and visualize the extent of the depletion region (Fig. 5) [240]. Advanced contactless techniques such as ultrafast optical microscopy have also been explored [266,267] to probe the detailed dynamics of charge carrier extraction. Further, using PL techniques to measure Fermi level splitting can give information about obtainable V_{OC} [221].
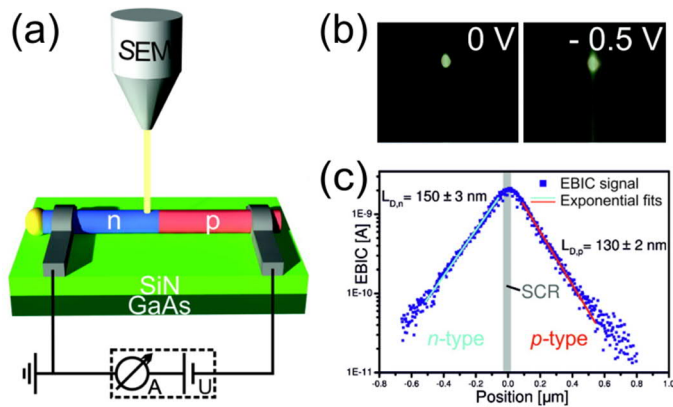
Figure 5 **Measuring nanowires by use of electron beam induced current (EBIC).** (a) A schematic showing the EBIC setup, used to measure on a single nanowire with an axial *p-n* junction. (b) EBIC images of an axial GaAs *p-n* nanowire (vertically oriented) measured under varying applied voltages. The EBIC signal creates a visualization of the extent of the depletion region, varying with applied voltage.

(c) EBIC signal along the nanowire axis. The minority carrier diffusion lengths of both electrons and holes are extracted by analyzing the exponential decay of the current signal. Reprinted (adapted) with permission from [240]. Copyright 2012 American Chemical Society.

Due to the strong geometry dependent absorption characteristics of nanowires, measurements performed on a single nanowire have limited relevance for nanowire array solar cells for measurements involving light interaction. Importantly, obtaining realistic *PCE* from single nanowire PV devices is difficult since the light concentration effects make the definition of an active area unclear [268], and such

measurements are difficult to standardize. Hence, to ensure fair comparisons between different approaches and efficiently advance the research field, *PCE* values are best obtained on full nanowire array solar cells under standardized conditions. If possible, the measurement should be performed by an institution providing certified *PCE* measurements [15], as pointed out by Beard et al. [10]. Table 1 shows a collection of reported performance metrics under 1 sun illumination for bottom-up synthesized III-V nanowire array solar cells, for junction geometries where the nanowires constitute the active region.

A common problem when measuring full nanowire arrays is to identify any contributions from single poorly performing nanowires or processing defects which can strongly affect the overall device performance. Both SPCM [238,269] and EBIC [270] have proved valuable to map out performance limiting areas of nanowire array devices. Also, it is important to rule out any contributions from the substrate to the generated photocurrent [125,271].

Nano-wire material	Patt-erning	Substrate	Growth method	Junction geometry doping order according to growth direction	Surface pas-sivation	PCE [%]	FF [%]	Jsc [mA/ cm^2]	Voc [V]	Array area [mm^2]	Ref.
GaAs	EBL	GaAs (111)B p	MOVPE, SA	radial p-n	Sulfur, ex situ	2.5	37.0	17.6	0.39	0.25	[238]
GaAs	EBL	Si (111) p	MBE, Ga	radial p-i-n	AlInP, in situ	3.3	46.5	18.2	0.39	0.01	[176]
GaAs	EBL	GaAs (111)B p	MOVPE, SA	radial p-n	InGaP, in situ	4.0	65.0	12.7	0.50	1.00	[252]
GaAs	EBL	GaAs (111)B n	MOVPE, SA	radial n-p	InGaP, in situ	6.6	62.0	24.3	0.44	0.25	[120]
GaAs	EBL	GaAs (111)B n	MOVPE, SA	radial n-i-p	InGaP in situ	7.4	69.0	18.9	0.57	0.25	[125]
GaAs	EBL	GaAs (111)B n	MOVPE, SA	axial n-i-p	None (BCB)	7.6	63.7	21.1	0.57	1.00	[111]
GaAs	NIL	GaAs (111)B p	MOVPE, Au	axial p-i-n	AlGaAs, in situ	15.3*	79.2	21.3	0.91	1.08	[17]
InP	EBL	InP (111)A p	MOVPE, SA	radial p-n	None (BCB)	3.4	57.0	13.7	0.43	15.6	[272]

Material	Lithography	Substrate	Growth	Junction	Passivation	PCE	FF	J_{SC}	V_{OC}		Ref.
InP	EBL	InP (111)A p	MOVPE, SA	radial p-n	NA	4.2	58.5	11.1	0.67	0.47	[178]
InP	NIL	InP (111)B p	MOVPE, Au	radial p-i-n	None (SiO$_x$)	5.3	67.7	15.7	0.50	0.01	[268]
InP	EBL	InP (111)A p	MOVPE, SA	radial p-n	AlInP, in situ (latt. mism.)	6.4	59.6	23.4	0.46	0.64	[177]
InP	NIL	InP (111)B p	MOVPE, Au	axial p-n	None (SiO$_x$)	11.1	73.0	21.0	0.73	0.25	[220]
InP	NIL	InP (111)B p	MOVPE, Au	axial p-i-n	None (SiO$_x$)	13.8*	72.4	24.6	0.78	1.00	[16]
InGaAs	none	multi-layer graphene	MOVPE, vdW	radial p-n	GaAs, in situ	2.5	55.3	17.2	0.26	5.10	[273]
InGaAs	EBL	GaAs (111)B p	MOVPE, SA	axial p-i-n	AlInP, in situ	7.1	72.1	18.2	0.54	0.81	[253]
Tandem											
GaAs on Si	UV-lith.	Si (111), n-p junct.	MOVPE, SA	axial n-i-p on Si	None (BCB)	11.4	57.8	20.6	0.96	1.00	[81]

Table 1 **Collection of reported performance metrics for bottom-up synthesized III-V nanowire array solar cells, measured under 1 sun illumination.** For nanowires with no intentional surface passivation, the layer closest to the nanowire surface is written in parentheses. Abbreviations: UV- ultraviolet, EBL- electron beam lithography, NIL- nanoimprint lithography, *PCE*- power conversion efficiency, *FF*- fill factor, J_{SC}- short circuit current, V_{OC}- open circuit voltage, MOVPE- metalorganic vapor phase epitaxy, SA- selective area, vdW- van der Waals epitaxy, NA- not available. An asterisk (*) by the PCE value indicates that the measurement is certified.

**Towards high efficiencies and low cost**

While impressive performance improvements have been achieved over the last years for nanowire solar cells, the best performing cells (Table 1) still have *PCE* values of only about half of the Shockley-

Queisser limit [109] and well below the planar counterparts for the different materials [3,15]. Also, while III-V solar cells have achieved the highest efficiencies to date in the planar architecture, their high cost prevents large-scale penetration of the terrestrial solar cell market. Thus there is a need to increase efficiency of III-V nanowire solar cells and develop cost-effective production methods.

Beyond the Shockley-Queisser limit

By optimizing single-junction nanowire solar cells as outlined in this review, e.g. in terms of surface passivation, junction design and crystal structure control, performance can be expected to improve towards planar counterparts and the Shockley-Queisser limit. In fact, it has been shown that nanowire solar cells can have a higher efficiency limit than a planar cell, since the nanowire geometry can suppress emission into some of the angles from which light is not incident, reducing entropy losses [274,275]. By utilizing such photonic design principles, the "conventional" Shockley-Queisser efficiency limit could be substantially surpassed [8]. Even higher efficiencies can potentially be achieved by applying a tandem approach. Here, solar cells of materials with different bandgaps are most commonly stacked on top of each other to absorb a larger part of the solar spectrum while reducing losses due to thermalization [56]. For III-V nanowire solar cells, two intuitive realizations of a tandem junction are illustrated in Fig. 6. In the first (Fig. 6a), two *p-n* junctions are placed within the same heterostructured nanowire, while in the second (Fig. 6b) the nanowire array is placed on top of a planar solar cell. These two basic architectures can of course also be expanded and combined to obtain more than two junctions.
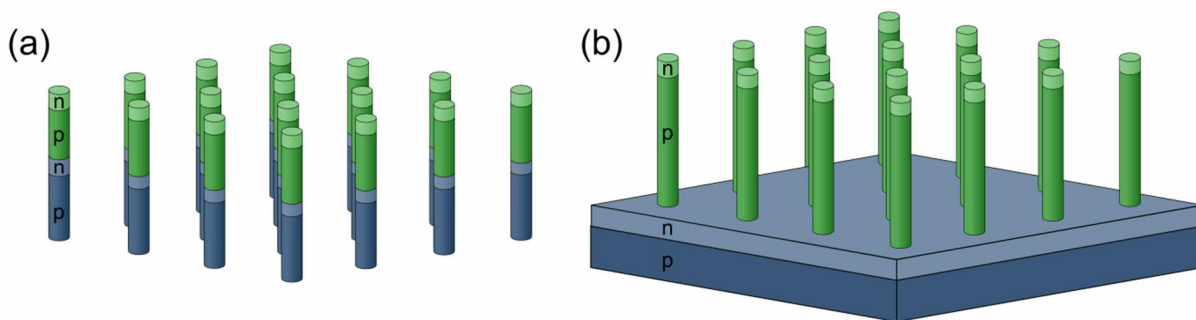
Figure 6   **Sketch of two basic nanowire based tandem solar cell structures**. (a) Arrays of heterostructured nanowires consisting of two materials of different bandgaps, each material consisting of a *p-n* junction. (b) Arrays of *p-n* junction nanowires on top of a planar solar cell. Blue and green indicate different materials, green having the higher bandgap.

Placing a III-V nanowire array on top of a conventional silicon solar cell (nanowire-on-Si) is especially appealing since it could potentially be integrated quite easily into the currently dominating Si solar cell industry, and possibly even put as an add on to already installed Si PV. Nanowire-on-Si solar cells have been theoretically studied by several authors [114,215,276–278]. To achieve maximum efficiency, the bandgap of the nanowire sub-cell should be approximately 1.7 eV in a double junction [114,215,276], or a combination of 1.5 and 2.0 eV in a triple junction [279]. This is achievable by the use of ternary III-V alloys such as $In_xGa_{1-x}P$ or $GaAs_yP_{1-y}$.

To optimize a nanowire based tandem cell, most of the aspects discussed so far in this review still apply to achieve good efficiencies, but some additional challenges arise. First, the total current in a series connected tandem cell is limited to the lowest current in any of the sub-cells. Therefore, the highest overall efficiency is achieved when the current generated in each sub-cell is the same (and maximized), known as the current-matching condition. In traditional thin-film tandem junctions, current-matching is obtained by adjusting the thicknesses of the different sub-cells. In a nanowire based tandem cell on the other hand, definition of array pitch, nanowire diameter and nanowire length independently or simultaneously can result in current-matching [215,277,279]. Tuning absorption by use of a dielectric shell could also be used to achieve current matching [124]. Second, a low-resistance tunnel junction is required to connect the sub-cells, capable of handling the potentially large current densities in the nanowires due to the inherent optical concentration [190]. Tunnel junctions have been realized within nanowire homostructures [255,280,281] and heterostructures [282,283], as well as between planar Si and InAs or InGaAs nanowires [284,285]. However, tunnel junctions between materials of relevant bandgaps to solar energy harvesting have not yet

been demonstrated in nanowires. Another possibility is to place the tunnel junction within the top part of the Si bottom cell [286]. We note that by connecting the sub-cells individually instead of in series, the current-matching requirement and need for tunnel junctions are no longer necessary, at the cost of losing the advantage of voltage addition from the sub-cells.

Heterojunction nanowire-on-Si solar cells has been realized between p-type Si and n-type InGaAs, InAs or InAsP nanowires [287–289], but these showed relatively low efficiencies. Similar low efficiencies were obtained in preliminary GaAsP nanowire-on-Si tandem devices [290]. Recently, Yao et al. [81] demonstrated a selective area grown GaAs n-i-p nanowire array on top of a Si cell, in which they saw voltage addition and a total efficiency of 11.4 %, better than each of the subcells (Fig. 7). This is an encouraging indicator that high efficiencies can be achieved in the nanowire-on-Si architecture, since as Yao et al. [81] points out; they had a poorly understood nanowire-Si heterointerface, un-passivated GaAs nanowires, non-optimized Si bottom cell and a sub-optimal bandgap combination.
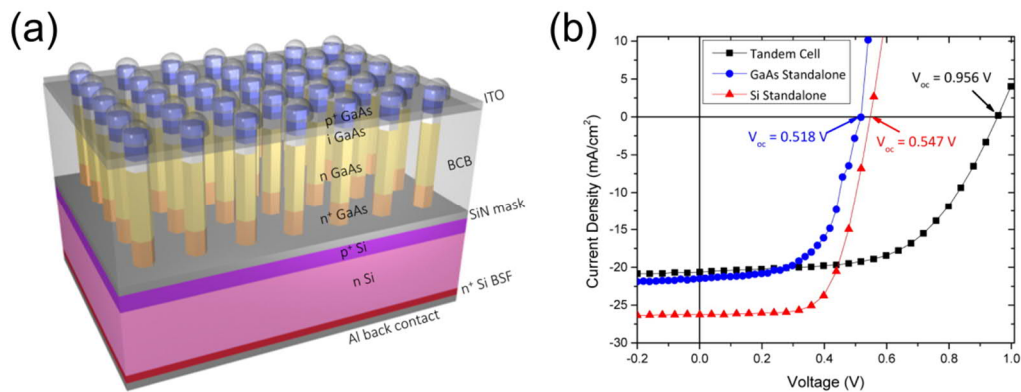
Figure 7 **GaAs nanowire-on-Si tandem solar cell.** (a) Schematic of the structure. (b) Current-voltage (J-V) curves showing open circuit voltage (V_{OC}) addition. J-V curves of the GaAs nanowire-on-Si tandem solar cell (black), the stand-alone GaAs nanowire cell (blue) and the stand-alone Si cell (red). The arrows indicate the V_{OC} for each cell, showing an addition of V_{OC} of the tandem cell (0.956 V) compared to separate stand-alone GaAs nanowire (0.518 V) and stand-alone Si (0.547 V) cells. Reprinted (adapted) with permission from [81]. Copyright 2015, American Chemical Society.

By the use of external light concentration, a further improvement of *PCE* might be expected (while also reducing material need) [291]. However, reported performance for nanowire array solar cells under concentrated light has so far not shown substantial improvements [16,220], and this effect needs to be better understood. For a single GaAsP nanowire PV device, a larger than expected efficiency increase was seen up to concentrations of at least 25 suns, attributed to a change in the recombination processes dominating the device [292]. Modelling indicate that the temperature rise in a nanowire solar cell should not be bigger than for planar counterparts [293], but external concentration and hence higher current densities are expected to raise demands on electrical contact quality [276,292].

Potential for cost reductions

The cost of III-V nanowire solar cells could be reduced as compared to planar cells due to the mere fact that only about 5 % of the expensive III-V material, as compared to a thin film, is needed to absorb almost all the sunlight [16,119]. However, as long as the nanowires are grown on III-V substrates, the substrate cost will be too high for large scale implementation. An interesting possibility is to remove the nanowires from the growth substrate using a polymer membrane that can be delaminated [294–297], which combined with selective-area growth, self-catalyzed growth or growth from metal particles defined by electrodeposition [298] would allow for substrate reuse and thus significant cost savings [299]. The membrane with the embedded nanowires could potentially act as a stand-alone flexible solar cell, or be used as part of a tandem structure. Another possibility to reduce the substrate cost is to grow the nanowires on a foreign cheap substrate, as discussed earlier. Using an entirely different approach, Heurlin et al. presented a substrate free nanowire growth method called Aerotaxy [300]. Here, nanowires are grown with extremely high growth rates from aerosol particles in a continuous flow of gas, avoiding limitations of batch-based synthesis methods which are currently one of the main cost drivers in III-V materials manufacturing [301].

Using this technique, both p-doping in GaAs nanowires [302] and compositional tuning in GaAsP nanowires [303] have been successfully demonstrated.

Summary and Outlook

Encouraging progress has been made in nanowire solar cell research over the last decade, with an impressive development in *PCE* for III-V nanowire array solar cells (Table 1). In this review we have summarized key design parameters that have been identified to optimize performance. With low material use, high absorption is possible in these structures by tuning geometry dependent resonant absorption characteristics, as predicted by theory and confirmed by experiments. However, the biggest challenge is the high level of synthesis control needed to obtain uniform arrays of nanowires with optimized charge carrier separation and collection properties. Further efforts are needed to optimize the nanowire array solar cells simultaneously in terms of key parameters discussed in this review; doping, crystal structure, surface passivation and contact formation. To achieve this, uniform and reproducible nanowire array growth from patterned substrates is essential. For efficient growth development and further understanding, a strong suit of characterization tools is needed. We believe it will be especially important to establish how results from fast and easy characterization techniques relate to performance of fully processed arrays. Until now, the devices with the highest reported *PCE*s have had an axial *p-n* junction geometry, while the solar cells based on radial *p-n* junctions have shown relatively low V_{OC}, seemingly suffering from poor junction quality.

To advance nanowire based solar cells towards possible commercialization the *PCE* needs to be increased, for which the tandem architecture is highly interesting. Especially interesting is the possibility of nanowire-on-Si tandem solar cells, with the first devices already successfully realized. Further cost reduction is also needed, especially when it comes to substrate cost and cost-efficient manufacturing methods for growth. We note that if III-V nanowire solar cells are to be implemented on a large scale, proper encapsulation and systems for handling and recycling of material are needed, due to the toxicity and high

cost of some of the elements. Rigorous testing will also be needed to evaluate long-term stability and reliability under outdoor operation conditions.

In conclusion, a strong and continued research effort is motivated, and required, to realize the full potential of nanowire based solar cells.

REFERENCES

[1]   S. Chu, A. Majumdar, Nature 488 (2012) 294–303.

[2]   ©Fraunhofer ISE Photovoltaics Report, Updat. 6 June 2016 (2016)
        https://www.ise.fraunhofer.de/en/.

[3]   A. Polman, M. Knight, E.C. Garnett, B. Ehrler, W.C. Sinke, Science 352 (2016)
        10.1126/science.aad4424.

[4]   N.S. Lewis, Science 351 (2016) 10.1126/science.aad1920.

[5]   M.A. Green, Third Generation Photovoltaics, Springer, New York, 2006.

[6]   G. Conibeer, Mater. Today 10 (2007) 42–50.

[7]   D. Ginley, R. Collins, M. Green, MRS Bull. 33 (2008) 355–364.

[8]   A. Polman, H.A. Atwater, Nat. Mater. 11 (2012) 174–177.

[9]   L. Tsakalakos, Mater. Sci. Eng. R Reports 62 (2008) 175–189.

[10]   M.C. Beard, J.M. Luther, A.J. Nozik, Nat. Nanotechnol. 9 (2014) 951–954.

[11]   N.P. Dasgupta, J. Sun, C. Liu, S. Brittman, S.C. Andrews, J. Lim, H. Gao, R. Yan, P. Yang, Adv. Mater. 26 (2014) 2137–2183.

[12]   Z. Fan, D.J. Ruebusch, A.A. Rathore, R. Kapadia, O. Ergen, P.W. Leu, A. Javey, Nano Res. 2 (2009) 829–843.

[13]   E.C. Garnett, M.L. Brongersma, Y. Cui, M.D. McGehee, Annu. Rev. Mater. Res. 41 (2011) 269–295.

[14]   R.R. LaPierre, A.C.E. Chia, S.J. Gibson, C.M. Haapamaki, J. Boulanger, R. Yee, P. Kuyanov, J. Zhang, N. Tajik, N. Jewell, K.M.A. Rahman, Phys. Status Solidi - Rapid Res. Lett. 7 (2013) 815–830.

[15]   M. Green, K. Emery, Prog. Photovolt Res. Appl. 24 (2016) 3–11.

[16]   J. Wallentin, N. Anttu, D. Asoli, M. Huffman, I. Åberg, M.H. Magnusson, G. Siefer, P. Fuss-Kailuweit, F. Dimroth, B. Witzigmann, H.Q. Xu, L. Samuelson, K. Deppert, M.T. Borgström, Science 339 (2013) 1057–1060.

[17]   I. Åberg, G. Vescovi, D. Asoli, U. Naseem, J.P. Gilboy, C. Sundvall, A. Dahlgren, K.E. Svensson,

N. Anttu, M.T. Björk, L. Samuelson, IEEE J. Photovoltaics 6 (2016) 185–190.

[18]   L. Tsakalakos, J. Balch, J. Fronheiser, B.A. Korevaar, O. Sulima, J. Rand, Appl. Phys. Lett. 91 (2007) 233117.

[19]   B. Tian, X. Zheng, T.J. Kempa, Y. Fang, N. Yu, G. Yu, J. Huang, C.M. Lieber, Nature 449 (2007) 885–889.

[20]   T.J. Kempa, B. Tian, D.R. Kim, H. Jinsong, Z. Xiaolin, C.M. Lieber, Nano Lett. 8 (2008) 3456–3460.

[21]   M.D. Kelzenberg, D.B. Turner-Evans, B.M. Kayes, M.A. Filier, M.C. Putnam, N.S. Lewis, H.A. Atwater, Nano Lett. 8 (2008) 710–714.

[22]   T. Stelzner, M. Pietsch, G. Andrä, F. Falk, E. Ose, S. Christiansen, Nanotechnology 19 (2008) 295203.

[23]   E.C. Garnett, P. Yang, J. Am. Chem. Soc. 130 (2008) 9224–9225.

[24]   M.D. Kelzenberg, S.W. Boettcher, J.A. Petykiewicz, D.B. Turner-Evans, M.C. Putnam, E.L. Warren, J.M. Spurgeon, R.M. Briggs, N.S. Lewis, H.A. Atwater, Nat. Mater. 9 (2010) 239–44.

[25]   K.-Q. Peng, S.-T. Lee, Adv. Mater. 23 (2011) 198–215.

[26]   C.E. Kendrick, J.M. Redwing, in:, Semicond. Nanowires Part B, 1st ed., Elsevier Inc., 2016, pp. 185–225.

[27]   J. Tang, Z. Huo, S. Brittman, H. Gao, P. Yang, Nat. Nanotechnol. 6 (2011) 568–572.

[28]   Z. Fan, H. Razavi, J. Do, A. Moriwaki, O. Ergen, Y.-L. Chueh, P.W. Leu, J.C. Ho, T. Takahashi, L.A. Reichertz, S. Neale, K. Yu, M. Wu, J.W. Ager, A. Javey, Nat. Mater. 8 (2009) 648–653.

[29]   J.-H. Im, J. Luo, M. Franckevičius, N. Pellet, P. Gao, T. Moehl, S.M. Zakeeruddin, M.K.

Nazeeruddin, M. Grätzel, N.-G. Park, Nano Lett. 15 (2015) 2120–2126.

[30]   Y.B. Tang, Z.H. Chen, H.S. Song, C.S. Lee, H.T. Cong, H.M. Cheng, W.J. Zhang, I. Bello, S.T. Lee, Nano Lett. 8 (2008) 4191–4195.

[31]   Y.J. Dong, B.Z. Tian, T.J. Kempa, C.M. Lieber, Nano Lett. 9 (2009) 2183–2187.

[32]   H.P.T. Nguyen, Y.L. Chang, I. Shih, Z. Mi, IEEE J. Sel. Top. Quantum Electron. 17 (2011) 1062–1069.

[33]   L.E. Jensen, M.T. Björk, S. Jeppesen, A.I. Persson, B.J. Ohlsson, L. Samuelson, Nano Lett. 4 (2004) 1961–1964.

[34]   A.M. Morales, C.M. Lieber, Science 279 (1998) 208–211.

[35]   B.H.-M. Kim, D.S. Kim, Y.S. Park, Adv. Mater. 14 (2002) 991–993.

[36]   K.A. Dick, Prog. Cryst. Growth Charact. Mater. 54 (2008) 138–173.

[37]   B.A. Wacaser, K.A. Dick, J. Johansson, M.T. Borgström, K. Deppert, L. Samuelson, Adv. Mater. 21 (2009) 153–165.

[38]   S. Barth, F. Hernandez-Ramirez, J.D. Holmes, A. Romano-Rodriguez, Prog. Mater. Sci. 55 (2010) 563–627.

[39]   R.S. Wagner, W.C. Ellis, Appl. Phys. Lett. 4 (1964) 89–90.

[40]   A.I. Persson, M.W. Larsson, S. Stenström, B.J. Ohlsson, L. Samuelson, L.R. Wallenberg, Nat. Mater. 3 (2004) 677–81.

[41]   S. Kodambaka, J. Tersoff, M.C. Reuter, F.M. Ross, Science 316 (2007) 729–32.

[42]   K.A. Dick, P. Caroff, Nanoscale 6 (2014) 3006–3021.

[43] C. Colombo, D. Spirkoska, M. Frimmer, G. Abstreiter, A. Fontcuberta i Morral, Phys. Rev. B 77 (2008) 155326.

[44] J. Motohisa, J. Takeda, M. Inari, J. Noborisaka, T. Fukui, Phys. E Low-Dimensional Syst. Nanostructures 23 (2004) 298–304.

[45] K. Tomioka, K. Ikejiri, T. Tanaka, J. Motohisa, S. Hara, K. Hiruma, T. Fukui, J. Mater. Res. 26 (2011) 2127–2141.

[46] K. Ikejiri, J. Noborisaka, S. Hara, J. Motohisa, T. Fukui, J. Cryst. Growth 298 (2007) 616–619.

[47] M.T. Björk, B.J. Ohlsson, T. Sass, A.I. Persson, C. Thelander, M.H. Magnusson, K. Deppert, L.R. Wallenberg, L. Samuelson, Appl. Phys. Lett. 80 (2002) 1058–1060.

[48] M.S. Gudiksen, L.J. Lauhon, J. Wang, D.C. Smith, C.M. Lieber, Nature 415 (2002) 617–620.

[49] Y. Wu, R. Fan, P. Yang, Nano Lett. 2 (2002) 83–86.

[50] G. Kästner, U. Gösele, Philos. Mag. 84 (2004) 3803–3824.

[51] F. Glas, Phys. Rev. B 74 (2006) 121302.

[52] L.J. Lauhon, M.S. Gudiksen, D. Wang, C.M. Lieber, Nature 420 (2002) 57–61.

[53] J. Johansson, K.A. Dick, CrystEngComm 13 (2011) 7175–7184.

[54] J.K. Hyun, S. Zhang, L.J. Lauhon, Annu. Rev. Mater. Res. 43 (2013) 451–479.

[55] S.A. Fortuna, X. Li, Semicond. Sci. Technol. 25 (2010) 24005.

[56] J.M. Olson, D.J. Friedman, S. Kurtz, in:, A. Luque, S. Hegedus (Eds.), Handb. Photovolt. Sci. Eng., 1st ed., John Wiley & Sons, Ltd, 2005, pp. 359–411.

[57] T. Mårtensson, C.P.T. Svensson, B.A. Wacaser, M.W. Larsson, W. Seifert, K. Deppert, A.

Gustafsson, L.R. Wallenberg, L. Samuelson, Nano Lett. 4 (2004) 1987–1990.

[58]   E.P.A.M. Bakkers, M.T. Borgström, M.A. Verheijen, MRS Bull. 32 (2007) 117–122.

[59]   K. Ikejiri, F. Ishizaka, K. Tomioka, T. Fukui, Nanotechnology 24 (2013) 115304.

[60]   M. Borg, H. Schmid, K.E. Moselund, G. Signorello, L. Gignac, J. Bruley, C. Breslin, P. Das
        Kanungo, P. Werner, H. Riel, Nano Lett. 14 (2014) 1914–1920.

[61]   M.A. Verheijen, G. Immink, T. De Smet, M.T. Borgström, E.P.A.M. Bakkers, J. Am. Chem. Soc.
        128 (2006) 1353–1359.

[62]   V. Dhaka, T. Haggren, H. Jussila, H. Jiang, E. Kauppinen, T. Huhtio, Nano Lett. 12 (2012) 1912–
        1918.

[63]   Y. Cohin, O. Mauguin, L. Largeau, G. Patriarche, F. Glas, E. Søndergård, J.C. Harmand, Nano
        Lett. 13 (2013) 2743–2747.

[64]   A.M. Munshi, D.L. Dheeraj, V.T. Fauske, D.C. Kim, A.T.J. Van Helvoort, B.O. Fimland, H.
        Weman, Nano Lett. 12 (2012) 4570–4576.

[65]   Y.J. Hong, W.H. Lee, Y. Wu, R.S. Ruoff, T. Fukui, Nano Lett. 12 (2012) 1431–1436.

[66]   A.M. Munshi, H. Weman, Phys. Status Solidi - Rapid Res. Lett. 7 (2013) 713–726.

[67]   J. Wallentin, D. Kriegner, J. Stangl, M.T. Borgström, Nano Lett. 14 (2014) 1707–1713.

[68]   A.R. Madaria, M. Yao, C. Chi, N. Huang, C. Lin, R. Li, M.L. Povinelli, P.D. Dapkus, C. Zhou,
        Nano Lett. 12 (2012) 2839–2845.

[69]   H.J. Fan, P. Werner, M. Zacharias, Small 2 (2006) 700–717.

[70]   T. Mårtensson, M.T. Borgström, W. Seifert, B.J. Ohlsson, L. Samuelson, Nanotechnology 14
        (2003) 1255–1258.

[71]   J. Motohisa, J. Noborisaka, J. Takeda, M. Inari, T. Fukui, J. Cryst. Growth 272 (2004) 180–185.

[72]   A.L. Roest, M.A. Verheijen, O. Wunnicke, S. Serafin, H. Wondergem, E.P.A.M. Bakkers, Nanotechnology 17 (2006) S271.

[73]   B. Bauer, A. Rudolph, M. Soda, A. Fontcuberta i Morral, J. Zweck, D. Schuh, E. Reiger, Nanotechnology 21 (2010) 435601.

[74]   D. Rudolph, L. Schweickert, S. Morkötter, B. Loitsch, S. Hertenberger, J. Becker, M. Bichler, G. Abstreiter, J.J. Finley, G. Koblmüller, Appl. Phys. Lett. 105 (2014) 33111.

[75]   T. Mårtensson, P. Carlberg, M.T. Borgström, L. Montelius, W. Seifert, L. Samuelson, Nano Lett. 4 (2004) 699–702.

[76]   A. Pierret, M. Hocevar, S.L. Diedenhofen, R.E. Algra, E. Vlieg, E.C. Timmering, M.A. Verschuuren, G.W.G. Immink, M.A. Verheijen, E.P.A.M. Bakkers, Nanotechnology 21 (2010) 65305.

[77]   S. Hertenberger, S. Funk, K. Vizbaras, A. Yadav, D. Rudolph, J. Becker, S. Bolte, M. Döblinger, M. Bichler, G. Scarpa, P. Lugli, I. Zardo, J.J. Finley, M.-C. Amann, G. Abstreiter, G. Koblmüller, Appl. Phys. Lett. 101 (2012) 43116.

[78]   A.M. Munshi, D.L. Dheeraj, V.T. Fauske, D.-C. Kim, J. Huh, J.F. Reinertsen, L. Ahtapodov, K. Lee, B. Heidari, A. van Helvoort, B.-O. Fimland, H. Weman, Nano Lett. 14 (2014) 960–966.

[79]   G. Otnes, M. Heurlin, M. Graczyk, J. Wallentin, D. Jacobsson, A. Berg, I. Maximov, M.T. Borgström, Nano Res. 9 (2016) 2852–2861.

[80]   M.C. Traub, W. Longsine, V.N. Truskett, Annu. Rev. Chem. Biomol. Eng. 7 (2016) 583–604.

[81]   M. Yao, S. Cong, S. Arab, N. Huang, M.L. Povinelli, S.B. Cronin, P.D. Dapkus, C. Zhou, Nano Lett. 15 (2015) 7217–7224.

[82]   D.S. Kim, R. Ji, H.J. Fan, F. Bertram, R. Scholz, A. Dadgar, K. Nielsch, A. Krost, J. Christen, U.

        Gösele, M. Zacharias, Small 3 (2007) 76–80.

[83]   C. Kauppinen, T. Haggren, A. Kravchenko, H. Jiang, T. Huhtio, E. Kauppinen, V. Dhaka, S.

        Suihkonen, M. Kaivola, H. Lipsanen, M. Sopanen, Nanotechnology 27 (2016) 135601.

[84]   B. Fuhrmann, H.S. Leipner, H.-R. Höche, L. Schubert, P. Werner, U. Gösele, Nano Lett. 5 (2005)

        2524–2527.

[85]   Y. Huang, T.W. Kim, S. Xiong, L.J. Mawst, T.F. Kuech, P.F. Nealey, Y. Dai, Z. Wang, W. Guo,

        D. Forbes, S.M. Hubbard, M. Nesnidal, Nano Lett. 13 (2013) 5979–5984.

[86]   L. Cao, J.S. White, J.-S. Park, J.A. Schuller, B.M. Clemens, M.L. Brongersma, Nat. Mater. 8

        (2009) 643–647.

[87]   L. Cao, P. Fan, A.P. Vasudev, J.S. White, Z. Yu, W. Cai, J.A. Schuller, S. Fan, M.L. Brongersma,

        Nano Lett. 10 (2010) 439–445.

[88]   P.M. Wu, N. Anttu, H.Q. Xu, L. Samuelson, M.E. Pistol, Nano Lett. 12 (2012) 1990–1995.

[89]   S.K. Kim, R.W. Day, J.F. Cahoon, T.J. Kempa, K.D. Song, H.G. Park, C.M. Lieber, Nano Lett. 12

        (2012) 4971–4976.

[90]   J. Svensson, N. Anttu, N. Vainorius, B.M. Borg, L.E. Wernersson, Nano Lett. 13 (2013) 1380–

        1385.

[91]   M.L. Brongersma, Y. Cui, S. Fan, Nat. Mater. 13 (2014) 451–60.

[92]   C. Lin, M.L. Povinelli, Opt. Express 17 (2009) 19371.

[93]   J. Kupec, R.L. Stoop, B. Witzigmann, Opt. Express 18 (2010) 27589–27605.

[94]   L. Wen, Z. Zhao, X. Li, Y. Shen, H. Guo, Y. Wang, Appl. Phys. Lett. 99 (2011) 2009–2012.

[95]   Z. Gu, P. Prete, N. Lovergine, B. Nabet, J. Appl. Phys. 109 (2011) 64314.

[96]   N. Huang, C. Lin, M.L. Povinelli, J. Opt. 14 (2012) 24004.

[97]   P. Krogstrup, H.I. Jørgensen, M. Heiss, O. Demichel, J. V Holm, M. Aagesen, J. Nygard, A. Fontcuberta i Morral, Nat. Photonics 7 (2013) 306–310.

[98]   K. Peng, Y. Xu, Y. Wu, Y. Yan, S.T. Lee, J. Zhu, Small 1 (2005) 1062–1067.

[99]   L. Tsakalakos, J. Balch, J. Fronheiser, M.-Y. Shih, S.F. LeBoeuf, M. Petrzykowski, P.J. Codella, B.A. Korevaar, O. Sulima, J. Rand, A. Davuluru, U. Rapol, J. Nanophotonics 1 (2007) 13552.

[100] L. Hu, G. Chen, Nano Lett. 7 (2007) 3249–3252.

[101] J. Zhu, Z. Yu, G.F. Burkhard, C.M. Hsu, S.T. Connor, Y. Xu, Q. Wang, M. McGehee, S. Fan, J. Cui, Nano Lett. 9 (2009) 279–282.

[102] V. Sivakov, G. Andrä, A. Gawlik, A. Berger, J. Plentz, F. Falk, S.H. Christiansen, Nano Lett. 9 (2009) 1549–1554.

[103] E. Garnett, P. Yang, Nano Lett. 10 (2010) 1082–1087.

[104] B. Wang, P.W. Leu, Opt. Lett. 37 (2012) 3756–3758.

[105] P. Kailuweit, M. Peters, J. Leene, K. Mergenthaler, F. Dimroth, A.W. Bett, Prog. Photovolt Res. Appl. 20 (2012) 659–676.

[106] Y. Hu, R.R. LaPierre, M. Li, K. Chen, J.-J. He, J. Appl. Phys. 112 (2012) 104311.

[107] N. Anttu, H.Q. Xu, Opt. Express 21 (2013) A558.

[108] N. Dhindsa, A. Chia, J. Boulanger, I. Khodadad, R. LaPierre, S.S. Saini, Nanotechnology 25 (2014) 305303.

[109] W. Shockley, H.J. Queisser, J. Appl. Phys. 32 (1961) 510–519.

[110] B.C.P. Sturmberg, K.B. Dossou, L.C. Botten, A.A. Asatryan, C.G. Poulton, R.C. McPhedran, C.M. de Sterke, ACS Photonics 1 (2014) 683–689.

[111] M. Yao, N. Huang, S. Cong, C. Chi, M.A. Seyedi, Y. Lin, Y. Cao, M.L. Povinelli, P.D. Dapkus, C. Zhou, Nano Lett. 14 (2014) 3293–3303.

[112] A. Benali, J. Michallon, P. Regreny, E. Drouard, P. Rojo, N. Chauvin, D. Bucci, A. Fave, A. Kaminski-Cachopo, M. Gendry, Energy Procedia 60 (2014) 109–115.

[113] Z. Li, Y.C. Wenas, L. Fu, S. Mokkapati, H.H. Tan, C. Jagadish, IEEE J. Photovoltaics 5 (2015) 854–864.

[114] S. Bu, X. Li, L. Wen, X. Zeng, Y. Zhao, W. Wang, Y. Wang, Appl. Phys. Lett. 102 (2013).

[115] O.L. Muskens, J.G. Rivas, R.E. Algra, E.P.A.M. Bakkers, A. Lagendijk, Nano Lett. 8 (2008) 2638–2642.

[116] S.L. Diedenhofen, G. Vecchi, R.E. Algra, A. Hartsuiker, O.L. Muskens, G. Immink, E.P.A.M. Bakkers, W.L. Vos, J.G. Rivas, Adv. Mater. 21 (2009) 973–978.

[117] Z. Fan, R. Kapadia, P.W. Leu, X. Zhang, Y.L. Chueh, K. Takei, K. Yu, A. Jamshidi, A.A. Rathore, D.J. Ruebusch, M. Wu, A. Javey, Nano Lett. 10 (2010) 3823–3827.

[118] S.L. Diedenhofen, O.T.A. Janssen, G. Grzela, E.P.A.M. Bakkers, J. Gómez Rivas, ACS Nano 5 (2011) 2316–2323.

[119] N. Anttu, A. Abrand, D. Asoli, M. Heurlin, I. Åberg, L. Samuelson, M.T. Borgström, Nano Res. 7 (2014) 816–823.

[120] G. Mariani, A.C. Scofield, C.-H. Hung, D.L. Huffaker, Nat. Commun. 4 (2013) 1497.

[121] J. Zhang, N. Dhindsa, A. Chia, J. Boulanger, I. Khodadad, S. Saini, R.R. LaPierre, Appl. Phys. Lett. 105 (2014) 2012–2016.

[122] J. Kupec, B. Witzigmann, Opt. Express 17 (2009) 10399–10410.

[123] N. Anttu, K.L. Namazi, P.M. Wu, P. Yang, H. Xu, H.Q. Xu, U. Håkanson, Nano Res. 5 (2012) 863–874.

[124] X. Li, T. Shi, G. Liu, L. Wen, B. Zhou, Y. Wang, Opt. Express 23 (2015) 25316–25328.

[125] G. Mariani, Z. Zhou, A. Scofield, D.L. Huffaker, Nano Lett. 13 (2013) 1632–1637.

[126] N. Anttu, H.Q. Xu, J. Nanosci. Nanotechnol. 10 (2010) 7183–7187.

[127] O.M. Ghahfarokhi, N. Anttu, L. Samuelson, I. Åberg, IEEE J. Photovoltaics (2016) 1–7.

[128] M. Koguchi, H. Kakibayashi, M. Yasawa, K. Hiruma, T. Katsuyama, Jpn. J. Appl. Phys. 31 (1992) 2061–2065.

[129] K. Hiruma, M. Yazawa, T. Katsuyama, K. Ogawa, K. Haraguchi, M. Koguchi, H. Kakibayashi, J. Appl. Phys. 77 (1995) 447–462.

[130] J. Johansson, L.S. Karlsson, C. Patrik T. Svensson, T. Mårtensson, B.A. Wacaser, K. Deppert, L. Samuelson, W. Seifert, Nat. Mater. 5 (2006) 574–580.

[131] P. Caroff, K.A. Dick, J. Johansson, M.E. Messing, K. Deppert, L. Samuelson, Nat. Nanotechnol. 4 (2009) 50–55.

[132] R.E. Algra, M.A. Verheijen, M.T. Borgström, L.-F. Feiner, G. Immink, W.J.P. van Enckevort, E. Vlieg, E.P.A.M. Bakkers, Nature 456 (2008) 369–372.

[133] J. Wallentin, K. Mergenthaler, M. Ek, L.R. Wallenberg, L. Samuelson, K. Deppert, M.-E. Pistol, M.T. Borgström, Nano Lett. 11 (2011) 2286–2290.

[134] H.J. Joyce, Q. Gao, H.H. Tan, C. Jagadish, Y. Kim, M.A. Fickenscher, S. Perera, T.B. Hoang, L.M. Smith, H.E. Jackson, J.M. Yarrison-Rice, X. Zhang, J. Zou, Adv. Funct. Mater. 18 (2008) 3794–3800.

[135] R.E. Algra, M.A. Verheijen, L.-F. Feiner, G.G.W. Immink, W.J.P. Van Enckevort, E. Vlieg, E.P.A.M. Bakkers, Nano Lett. 11 (2011) 1259–1264.

[136] P. Krogstrup, S. Curiotto, E. Johnson, M. Aagesen, J. Nygård, D. Chatain, Phys. Rev. Lett. 106 (2011) 125505.

[137] Y.C. Chou, K. Hillerich, J. Tersoff, M.C. Reuter, K.A. Dick, F.M. Ross, Science 343 (2014) 281–284.

[138] F. Glas, J.-C. Harmand, G. Patriarche, Phys. Rev. Lett. 99 (2007) 146101.

[139] V.G. Dubrovskii, N. V. Sibirev, Phys. Rev. B 77 (2008) 35414.

[140] V.G. Dubrovskii, N. V. Sibirev, J.C. Harmand, F. Glas, Phys. Rev. B 78 (2008) 235301.

[141] D. Jacobsson, F. Panciera, J. Tersoff, M.C. Reuter, S. Lehmann, S. Hofmann, K.A. Dick, F.M. Ross, Nature 531 (2016) 317–322.

[142] P. Parkinson, H.J. Joyce, Q. Gao, H.H. Tan, X. Zhang, J. Zou, C. Jagadish, L.M. Herz, M.B. Johnston, Nano Lett. 9 (2009) 3349–3353.

[143] M.D. Schroer, J.R. Petta, Nano Lett. 10 (2010) 1618–1622.

[144] C. Thelander, P. Caroff, S. Plissard, A.W. Dey, K.A. Dick, Nano Lett. 11 (2011) 2424–2429.

[145] J. Wallentin, M. Ek, L.R. Wallenberg, L. Samuelson, M.T. Borgström, Nano Lett. 12 (2012) 151–155.

[146] H.J. Joyce, J. Wong-Leung, C.K. Yong, C.J. Docherty, S. Paiman, Q. Gao, H.H. Tan, C. Jagadish,

J. Lloyd-Hughes, L.M. Herz, M.B. Johnston, Nano Lett. 12 (2012) 5325–5330.

[147]   K. Shimamura, Z. Yuan, F. Shimojo, A. Nakano, Appl. Phys. Lett. 103 (2013) 22105.

[148]   G. Bussone, H. Schäfer-Eberwein, E. Dimakis, A. Biermanns, D. Carbone, A. Tahraoui, L. Geelhaar, P. Haring Bolivar, T.U. Schülli, U. Pietsch, Nano Lett. 15 (2015) 981–989.

[149]   M. Fu, Z. Tang, X. Li, Z. Ning, D. Pan, J. Zhao, X. Wei, Q. Chen, Nano Lett. 16 (2016) 2478–2484.

[150]   M.C. Plante, R.R. LaPierre, Nanotechnology 19 (2008) 495603.

[151]   Y. Kitauchi, Y. Kobayashi, K. Tomioka, S. Hara, K. Hiruma, T. Fukui, J. Motohisa, Nano Lett. 10 (2010) 1699–1703.

[152]   D. Jacobsson, S. Lehmann, K.A. Dick, Nanoscale 6 (2014) 8257.

[153]   H.J. Joyce, Q. Gao, H.H. Tan, C. Jagadish, Y. Kim, X. Zhang, Y. Guo, J. Zou, Nano Lett. 7 (2007) 921–926.

[154]   J. Johansson, K.A. Dick, P. Caroff, M.E. Messing, J. Bolinsson, K. Deppert, L. Samuelson, J. Phys. Chem. C 114 (2010) 3837–3842.

[155]   T.T.T. Vu, T. Zehender, M.A. Verheijen, S.R. Plissard, G.W.G. Immink, J.E.M. Haverkort, E.P.A.M. Bakkers, Nanotechnology 24 (2013) 115705.

[156]   S. Assali, I. Zardo, S. Plissard, D. Kriegner, M.A. Verheijen, G. Bauer, A. Meijerink, A. Belabbes, F. Bechstedt, J.E.M. Haverkort, E.P.A.M. Bakkers, Nano Lett. 13 (2013) 1559–1563.

[157]   S. Lehmann, J. Wallentin, D. Jacobsson, K. Deppert, K.A. Dick, Nano Lett. 13 (2013) 4099–4105.

[158]   J. Wallentin, M.T. Borgström, J. Mater. Res. 26 (2011) 2142–2156.

[159]   K. Storm, F. Halvardsson, M. Heurlin, D. Lindgren, A. Gustafsson, P.M. Wu, B. Monemar, L.

Samuelson, Nat. Nanotechnol. 7 (2012) 718–22.

[160]   C. Blömers, T. Grap, M.I. Lepsa, J. Moers, S. Trellenkamp, D. Grützmacher, H. Lüth, T. Schäpers, Appl. Phys. Lett. 101 (2012) 152106.

[161]   D. Lindgren, O. Hultin, M. Heurlin, K. Storm, M.T. Borgström, L. Samuelson, A. Gustafsson, Nanotechnology 26 (2015) 45705.

[162]   O. Hultin, G. Otnes, M.T. Borgström, M. Björk, L. Samuelson, K. Storm, Nano Lett. 16 (2016) 205–211.

[163]   C. Liu, L. Dai, L.P. You, W.J. Xu, G.G. Qin, Nanotechnology 19 (2008) 465203.

[164]   F. Wang, Q. Gao, K. Peng, Z. Li, Z. Li, Y. Guo, L. Fu, L.M. Smith, H.H. Tan, C. Jagadish, Nano Lett. 15 (2015) 3017–3023.

[165]   M. Hilse, M. Ramsteiner, S. Breuer, L. Geelhaar, H. Riechert, Appl. Phys. Lett. 96 (2010) 2008–2011.

[166]   B. Ketterer, E. Uccelli, A. Fontcuberta i Morral, Nanoscale 4 (2012) 1789.

[167]   D.E. Perea, E.R. Hemesath, E.J. Schwalbach, J.L. Lensch-Falk, P.W. Voorhees, L.J. Lauhon, Nat. Nanotechnol. 4 (2009) 315–319.

[168]   N. Jeon, L.J. Lauhon, in:, Semicond. Semimetals, 1st ed., Elsevier Inc., 2015, pp. 249–278.

[169]   B. Tian, T.J. Kempa, C.M. Lieber, Chem. Soc. Rev. 38 (2009) 16–24.

[170]   A. Kandala, T. Betti, A. Fontcuberta i Morral, Phys. Status Solidi Appl. Mater. Sci. 206 (2009) 173–178.

[171]   S. Yu, B. Witzigmann, Opt. Express 21 (2013) A167.

[172]   S. Wang, X. Yan, X. Zhang, J. Li, X. Ren, Nanoscale Res. Lett. 10 (2015) 22.

[173] B.M. Kayes, H.A. Atwater, N.S. Lewis, J. Appl. Phys. 97 (2005) 114302.

[174] J.D. Christesen, X. Zhang, C.W. Pinion, T.A. Celano, C.J. Flynn, J.F. Cahoon, Nano Lett. 12 (2012) 6024–6029.

[175] A.C.E. Chia, R.R. LaPierre, J. Appl. Phys. 114 (2013) 74317.

[176] J.P. Boulanger, A.C.E. Chia, B. Wood, S. Yazdi, T. Kasama, M. Aagesen, R.R. LaPierre, IEEE J. Photovoltaics 6 (2016) 661–667.

[177] M. Yoshimura, E. Nakai, K. Tomioka, T. Fukui, Appl. Phys. Express 6 (2013) 52301.

[178] T. Fukui, M. Yoshimura, E. Nakai, K. Tomioka, Ambio 41 (2012) 119–124.

[179] J. Wallentin, M.E. Messing, E. Trygg, L. Samuelson, K. Deppert, M.T. Borgström, J. Cryst. Growth 331 (2011) 8–14.

[180] S. Gorji Ghalamestani, M. Heurlin, L.-E. Wernersson, S. Lehmann, K.A. Dick, Nanotechnology 23 (2012) 285601.

[181] F. Haas, K. Sladek, A. Winden, M. von der Ahe, T.E. Weirich, T. Rieger, H. Lüth, D. Grützmacher, T. Schäpers, H. Hardtdegen, Nanotechnology 24 (2013) 85603.

[182] J.B. Mullin, J. Cryst. Growth 42 (1977) 77–89.

[183] R. Bhat, C. Caneau, C.E. Zah, M.A. Koza, W.A. Bonner, D.M. Hwang, S.A. Schwarz, S.G. Menocal, F.G. Favire, J. Cryst. Growth 107 (1991) 772–778.

[184] M. Kondo, C. Anayama, T. Tanahashi, S. Yamazaki, J. Cryst. Growth 124 (1992) 449–456.

[185] J.A. Czaban, D.A. Thompson, R.R. LaPierre, Nano Lett. 9 (2008) 148–154.

[186] M. Heurlin, O. Hultin, K. Storm, D. Lindgren, M.T. Borgström, L. Samuelson, Nano Lett. 14 (2014) 749–753.

[187] K. Cho, D.J. Ruebusch, M.H. Lee, J.H. Moon, A.C. Ford, R. Kapadia, K. Takei, O. Ergen, A. Javey, Appl. Phys. Lett. 98 (2011) 203101.

[188] S. Yu, J. Kupec, B. Witzigmann, J. Comput. Theor. Nanosci. 9 (2012) 688–695.

[189] D. Liang, Y. Kang, Y. Huo, Y. Chen, Y. Cui, J.S. Harris, Nano Lett. 13 (2013) 4850–4856.

[190] M.T. Borgström, J. Wallentin, M. Heurlin, S. Fält, P. Wickert, J. Leene, M.H. Magnusson, K. Deppert, L. Samuelson, IEEE J. Sel. Top. Quantum Electron. 17 (2011) 1050–1061.

[191] M.T. Borgström, J. Wallentin, J. Trägårdh, P. Ramvall, M. Ek, L.R. Wallenberg, L. Samuelson, K. Deppert, Nano Res. 3 (2010) 264–270.

[192] D. Jacobsson, J.M. Persson, D. Kriegner, T. Etzelstorfer, J. Wallentin, J.B. Wagner, J. Stangl, L. Samuelson, K. Deppert, M.T. Borgström, Nanotechnology 23 (2012) 245601.

[193] A. Berg, K. Mergenthaler, M. Ek, M.-E. Pistol, L.R. Wallenberg, M.T. Borgström, Nanotechnology 25 (2014) 505601.

[194] G.E. Cirlin, A.D. Bouravleuv, I.P. Soshnikov, Y.B. Samsonenko, V.G. Dubrovskii, E.M. Arakcheeva, E.M. Tanklevskaya, P. Werner, Nanoscale Res. Lett. 5 (2010) 360–363.

[195] M. Yoshimura, E. Nakai, K. Tomioka, T. Fukui, Appl. Phys. Lett. 103 (2013) 243111.

[196] N. Han, F. Wang, S. Yip, J.J. Hou, F. Xiu, X. Shi, A.T. Hui, T. Hung, J.C. Ho, Appl. Phys. Lett. 101 (2012) 13105.

[197] N. Han, Z. Yang, F. Wang, G. Dong, S. Yip, X. Liang, T.F. Hung, Y. Chen, J.C. Ho, ACS Appl. Mater. Interfaces 7 (2015) 20454–20459.

[198] W.U. Huynh, J.J. Dittmer, A. Alivisatos, Science 295 (2002) 2425–2427.

[199] L.E. Greene, M. Law, B.D. Yuhas, P. Yang, J. Phys. Chem. C 111 (2007) 18451–18456.

[200] C.J. Novotny, E.T. Yu, P.K.L. Yu, Nano Lett. 8 (2008) 778–779.

[201] H. Bi, R.R. LaPierre, Nanotechnology 20 (2009) 465205.

[202] G. Mariani, Y. Wang, P.S. Wong, A. Lech, C.H. Hung, J. Shapiro, S. Prikhodko, M. El-Kady, R.B. Kaner, D.L. Huffaker, Nano Lett. 12 (2012) 3581–3586.

[203] M. Law, L.E. Greene, J.C. Johnson, R. Saykally, P.D. Yang, Nat. Mater. 4 (2005) 455–459.

[204] J.B. Baxter, E.S. Aydil, Appl. Phys. Lett. 86 (2005) 53114.

[205] M.Y. Song, Y.R. Ahn, S.M. Jo, D.Y. Kim, J.-P. Ahn, Appl. Phys. Lett. 87 (2005) 113113.

[206] S. Hu, C.-Y. Chi, K.T. Fountaine, M. Yao, H.A. Atwater, P.D. Dapkus, N.S. Lewis, C. Zhou, Energy Environ. Sci. 6 (2013) 1879–1890.

[207] J. Wu, Y. Li, J. Kubota, K. Domen, M. Aagesen, T. Ward, A. Sanchez, R. Beanland, Y. Zhang, M. Tang, S. Hatch, A. Seeds, H. Liu, Nano Lett. 14 (2014) 2013–2018.

[208] R. Kapadia, Z. Fan, A. Javey, Appl. Phys. Lett. 96 (2010) 103116.

[209] Y. Chen, P. Kivisaari, M.-E. Pistol, N. Anttu, Nanotechnology 27 (2016) 435404.

[210] A.H. Trojnar, C.E. Valdivia, K.M. Azizur-Rahman, R.R. LaPierre, K. Hinzer, J.J. Krich, in:, 2015 IEEE 42nd Photovolt. Spec. Conf., IEEE, 2015, pp. 1–6.

[211] A.H. Trojnar, C.E. Valdivia, R.R. LaPierre, K. Hinzer, J.J. Krich, arXiv.org (2016) 1–9.

[212] R.R. LaPierre, J. Appl. Phys. 109 (2011) 34311.

[213] T.J. Kempa, J.F. Cahoon, S.-K. Kim, R.W. Day, D.C. Bell, H.-G. Park, C.M. Lieber, Proc. Natl. Acad. Sci. 109 (2012) 1407–1412.

[214] M. Heurlin, N. Anttu, C. Camus, L. Samuelson, M.T. Borgström, Nano Lett. 15 (2015) 3597–

3602.

[215]   N. Huang, C. Lin, M.L. Povinelli, J. Appl. Phys. 112 (2012) 64321.

[216]   S. Yu, F. Roemer, B. Witzigmann, J. Photonics Energy 2 (2012) 28002.

[217]   X. Wang, M.R. Khan, M. Lundstrom, P. Bermel, Opt. Express 22 (2014) A344.

[218]   H.C. Casey, E. Buehler, Appl. Phys. Lett. 30 (1977) 247–249.

[219]   D.E. Aspnes, Surf. Sci. 132 (1983) 406–421.

[220]   Y. Cui, J. Wang, S.R. Plissard, A. Cavalli, T.T.T. Vu, R.P.J. van Veldhoven, L. Gao, M. Trainor,
         M.A. Verheijen, J.E.M. Haverkort, E.P.A.M. Bakkers, Nano Lett. 13 (2013) 4113–4117.

[221]   T.T.D. Tran, H. Sun, K.W. Ng, F. Ren, K. Li, F. Lu, E. Yablonovitch, C.J. Chang-Hasnain, Nano
         Lett. 14 (2014) 3235–3240.

[222]   H.J. Joyce, C.J. Docherty, Q. Gao, H.H. Tan, C. Jagadish, J. Lloyd-Hughes, L.M. Herz, M.B.
         Johnston, Nanotechnology 24 (2013) 214006.

[223]   O. Demichel, M. Heiss, J. Bleuse, H. Mariette, A. Fontcuberta i Morral, Appl. Phys. Lett. 97
         (2010) 201907.

[224]   C.-C. Chang, C.-Y. Chi, M. Yao, N. Huang, C.-C. Chen, J. Theiss, A.W. Bushmaker, S.
         LaLumondiere, T.-W. Yeh, M.L. Povinelli, C. Zhou, P.D. Dapkus, S.B. Cronin, Nano Lett. 12
         (2012) 4484–4489.

[225]   N. Jiang, P. Parkinson, Q. Gao, S. Breuer, H.H. Tan, J. Wong-Leung, C. Jagadish, Appl. Phys.
         Lett. 101 (2012) 23111.

[226]   A.C.E. Chia, M. Tirado, F. Thouin, R. Leonelli, D. Comedi, R.R. LaPierre, Semicond. Sci.
         Technol. 28 (2013) 105026.

[227] N. Sköld, L.S. Karlsson, M.W. Larsson, M.-E. Pistol, W. Seifert, J. Trägårdh, L. Samuelson, Nano Lett. 5 (2005) 1943–1947.

[228] A. Lin, J.N. Shapiro, P.N. Senanayake, A.C. Scofield, P.-S. Wong, B. Liang, D.L. Huffaker, Nanotechnology 23 (2012) 105701.

[229] A. Darbandi, S.P. Watkins, J. Appl. Phys. 120 (2016) 14301.

[230] L. V. Titova, T.B. Hoang, H.E. Jackson, L.M. Smith, J.M. Yarrison-Rice, Y. Kim, H.J. Joyce, H.H. Tan, C. Jagadish, Appl. Phys. Lett. 89 (2006) 173126.

[231] S. Perera, M.A. Fickenscher, H.E. Jackson, L.M. Smith, J.M. Yarrison-Rice, H.J. Joyce, Q. Gao, H.H. Tan, C. Jagadish, X. Zhang, J. Zou, Appl. Phys. Lett. 93 (2008) 53110.

[232] H.L. Zhou, T.B. Hoang, D.L. Dheeraj, A.T.J. van Helvoort, L. Liu, J.C. Harmand, B.O. Fimland, H. Weman, Nanotechnology 20 (2009) 415701.

[233] K. Tomioka, Y. Kobayashi, J. Motohisa, S. Hara, T. Fukui, Nanotechnology 20 (2009) 145302.

[234] N. Jiang, Q. Gao, P. Parkinson, J. Wong-Leung, S. Mokkapati, S. Breuer, H.H. Tan, C.L. Zheng, J. Etheridge, C. Jagadish, Nano Lett. 13 (2013) 5135–5140.

[235] A.C.E. Chia, M. Tirado, Y. Li, S. Zhao, Z. Mi, D. Comedi, R.R. LaPierre, J. Appl. Phys. 111 (2012) 94319.

[236] J. V Holm, H.I. Jørgensen, P. Krogstrup, J. Nygård, H. Liu, M. Aagesen, Nat. Commun. 4 (2013) 1498.

[237] T. Haggren, H. Jiang, J.-P. Kakko, T. Huhtio, V. Dhaka, E. Kauppinen, H. Lipsanen, Appl. Phys. Lett. 105 (2014) 33114.

[238] G. Mariani, P.S. Wong, A.M. Katzenmeyer, F. Léonard, J. Shapiro, D.L. Huffaker, Nano Lett. 11

(2011) 2490–2494.

[239] N. Tajik, A.C.E. Chia, R.R. LaPierre, Appl. Phys. Lett. 100 (2012) 2010–2013.

[240] C. Gutsche, R. Niepelt, M. Gnauck, A. Lysov, W. Prost, C. Ronning, F.J. Tegude, Nano Lett. 12 (2012) 1453–1458.

[241] P.A. Alekseev, M.S. Dunaevskiy, V.P. Ulin, T. V. Lvova, D.O. Filatov, A. V. Nezhdanov, A.I. Mashin, V.L. Berkovits, Nano Lett. 15 (2015) 63–68.

[242] L. Ahtapodov, J. Todorovic, P. Olk, T. Mjåland, P. Slåttnes, D.L. Dheeraj, A.T.J. Van Helvoort, B.O. Fimland, H. Weman, Nano Lett. 12 (2012) 6090–6095.

[243] H.J. Joyce, P. Parkinson, N. Jiang, C.J. Docherty, Q. Gao, H.H. Tan, C. Jagadish, L.M. Herz, M.B. Johnston, Nano Lett. 14 (2014) 5989–5994.

[244] W.M. Bullis, Solid. State. Electron. 9 (1966) 143–168.

[245] J.E. Allen, E.R. Hemesath, D.E. Perea, J.L. Lensch-Falk, Z.Y. Li, F. Yin, M.H. Gass, P. Wang, A.L. Bleloch, R.E. Palmer, L.J. Lauhon, Nat. Nanotechnol. 3 (2008) 168–173.

[246] D.E. Perea, J.E. Allen, S.J. May, B.W. Wessels, D.N. Seidman, L.J. Lauhon, Nano Lett. 6 (2006) 181–185.

[247] M. Bar-Sadan, J. Barthel, H. Shtrikman, L. Houben, Nano Lett. 12 (2012) 2352–2356.

[248] M.J. Tambe, S. Ren, S. Gradečak, Nano Lett. 10 (2010) 4584–4589.

[249] S. Breuer, C. Pfüller, T. Flissikowski, O. Brandt, H.T. Grahn, L. Geelhaar, H. Riechert, Nano Lett. 11 (2011) 1276–1279.

[250] F. Léonard, A.A. Talin, Nat. Nanotechnol. 6 (2011) 773–783.

[251] A.C.E. Chia, R.R. LaPierre, Nanotechnology 22 (2011) 245304.

[252] E. Nakai, M. Yoshimura, K. Tomioka, T. Fukui, Jpn. J. Appl. Phys. 52 (2013) 55002.

[253] E. Nakai, M. Chen, M. Yoshimura, K. Tomioka, T. Fukui, Jpn. J. Appl. Phys. 54 (2015) 15201.

[254] J. Zhang, A.C.E. Chia, R.R. LaPierre, Semicond. Sci. Technol. 29 (2014) 54002.

[255] J. Wallentin, P. Wickert, M. Ek, A. Gustafsson, L. Reine Wallenberg, M.H. Magnusson, L. Samuelson, K. Deppert, M.T. Borgström, Appl. Phys. Lett. 99 (2011) 253105.

[256] M. Tchernycheva, L. Rigutti, G. Jacopin, A. de Luna Bugallo, P. Lavenus, F.H. Julien, M. Timofeeva, A.D. Bouravleuv, G.E. Cirlin, V. Dhaka, H. Lipsanen, L. Largeau, Nanotechnology 23 (2012) 265402.

[257] P. Lavenus, A. Messanvi, L. Rigutti, A. De Luna Bugallo, H. Zhang, F. Bayle, F.H. Julien, J. Eymery, C. Durand, M. Tchernycheva, Nanotechnology 25 (2014) 255201.

[258] P. Tchoulfian, F. Donatini, F. Levy, A. Dussaigne, P. Ferret, J. Pernot, Nano Lett. 14 (2014) 3491–3498.

[259] Z. Zhong, Z. Li, Q. Gao, Z. Li, K. Peng, L. Li, S. Mokkapati, K. Vora, J. Wu, G. Zhang, Z. Wang, L. fu, H.H. Tan, C. Jagadish, Nano Energy 28 (2016) 106–114.

[260] A. Gustafsson, J. Bolinsson, N. Sköld, L. Samuelson, Appl. Phys. Lett. 97 (2010) 72114.

[261] J. Bolinsson, K. Mergenthaler, L. Samuelson, A. Gustafsson, J. Cryst. Growth 315 (2011) 138–142.

[262] C. Colombo, M. Heiβ, M. Grätzel, A. Fontcuberta i Morral, Appl. Phys. Lett. 94 (2009) 173108.

[263] R. Graham, C. Miller, E. Oh, D. Yu, Nano Lett. 11 (2011) 717–722.

[264] C. Gutsche, A. Lysov, D. Braam, I. Regolin, G. Keller, Z.A. Li, M. Geller, M. Spasova, W. Prost, F.J. Tegude, Adv. Funct. Mater. 22 (2012) 929–936.

[265] P. Parkinson, Y.H. Lee, L. Fu, S. Breuer, H.H. Tan, C. Jagadish, Nano Lett. 13 (2013) 1405–1409.

[266] M.A. Seo, J. Yoo, S.A. Dayeh, S.T. Picraux, A.J. Taylor, R.P. Prasankumar, Nano Lett. 12 (2012) 6334–6338.

[267] M.M. Gabriel, E.M. Grumstrup, J.R. Kirschbrown, C.W. Pinion, J.D. Christesen, D.F. Zigler, E.E.M. Cating, J.F. Cahoon, J.M. Papanikolas, Nano Lett. 14 (2014) 3079–3087.

[268] A. Nowzari, M. Heurlin, V. Jain, K. Storm, A. Hosseinnia, N. Anttu, M.T. Borgström, H. Pettersson, L. Samuelson, Nano Lett. 15 (2015) 1809−1814.

[269] S.L. Howell, S. Padalkar, K. Yoon, Q. Li, D.D. Koleske, J.J. Wierer, G.T. Wang, L.J. Lauhon, Nano Lett. 13 (2013) 5123–5128.

[270] L. Yu, L. Rigutti, M. Tchernycheva, S. Misra, M. Foldyna, G. Picardi, P. Roca i Cabarrocas, Nanotechnology 24 (2013) 275401.

[271] V. Jain, A. Nowzari, J. Wallentin, M.T. Borgström, M.E. Messing, D. Asoli, M. Graczyk, B. Witzigmann, F. Capasso, L. Samuelson, H. Pettersson, Nano Res. 7 (2014) 544–552.

[272] H. Goto, K. Nosaki, K. Tomioka, S. Hara, K. Hiruma, J. Motohisa, T. Fukui, Appl. Phys. Express 2 (2009) 35004.

[273] P.K. Mohseni, A. Behnam, J.D. Wood, X. Zhao, K.J. Yu, N.C. Wang, A. Rockett, J.A. Rogers, J.W. Lyding, E. Pop, X. Li, Adv. Mater. 26 (2014) 3755–3760.

[274] N. Anttu, ACS Photonics 2 (2015) 446–453.

[275] Y. Xu, T. Gong, J.N. Munday, Sci. Rep. 5 (2015) 13536.

[276] R.R. LaPierre, J. Appl. Phys. 110 (2011) 14310.

[277] Y. Hu, M. Li, J.-J. He, R.R. LaPierre, Nanotechnology 24 (2013) 65402.

[278] Y. Wang, Y. Zhang, D. Zhang, S. He, X. Li, Nanoscale Res. Lett. 10 (2015) 269.

[279] L. Wen, X. Li, Z. Zhao, S. Bu, X. Zeng, J. Huang, Y. Wang, Nanotechnology 23 (2012) 505202.

[280] M. Heurlin, P. Wickert, S. Fält, M.T. Borgström, K. Deppert, L. Samuelson, M.H. Magnusson, Nano Lett. 11 (2011) 2028–2031.

[281] A. Darbandi, K.L. Kavanagh, S.P. Watkins, Nano Lett. 15 (2015) 5408–5413.

[282] J. Wallentin, J.M. Persson, J.B. Wagner, L. Samuelson, K. Deppert, M.T. Borgström, Nano Lett. 10 (2010) 974–979.

[283] B.M. Borg, K.A. Dick, B. Ganjipour, M.E. Pistol, L.E. Wernersson, C. Thelander, Nano Lett. 10 (2010) 4080–4085.

[284] C.D. Bessire, M.T. Björk, H. Schmid, A. Schenk, K.B. Reuter, H. Riel, Nano Lett. 11 (2011) 4195–4199.

[285] T. Yang, S. Hertenberger, S. Morkötter, G. Abstreiter, G. Koblmüller, Appl. Phys. Lett. 101 (2012) 233102.

[286] J. Yang, J. Goguen, R. Kleiman, IEEE Electron Device Lett. 33 (2012) 1732–1734.

[287] W. Wei, X.Y. Bao, C. Soci, Y. Ding, Z.L. Wang, D. Wang, Nano Lett. 9 (2009) 2926–2934.

[288] J.C. Shin, K.H. Kim, K.J. Yu, H. Hu, L. Yin, C.Z. Ning, J.A. Rogers, J.M. Zuo, X. Li, Nano Lett. 11 (2011) 4831–4838.

[289] J.C. Shin, A. Lee, P.K. Mohseni, D.Y. Kim, L. Yu, J.H. Kim, H.J. Kim, (2013) 5463–5471.

[290] J. V Holm, M. Aagesen, Y. Zhang, J. Wu, S. Hatch, H. Liu, in:, 2014 IEEE 40th Photovolt. Spec. Conf., IEEE, 2014, pp. 1041–1044.

[291] M.A. Green, in:, Sol. Cells, The University of New South Wales, Kensington, NSW 2033, 1982,

pp. 204–221.

[292] M. Aagesen, J. V. Holm, H.I. Jorgensen, H. Liu, Conf. Rec. IEEE Photovolt. Spec. Conf. (2013) 254–257.

[293] S.-H. Wu, M.L. Povinelli, Opt. Express 23 (2015) A1363.

[294] J.M. Spurgeon, K.E. Plass, B.M. Kayes, B.S. Brunschwig, H.A. Atwater, N.S. Lewis, Appl. Phys. Lett. 93 (2008) 32112.

[295] A.J. Standing, S. Assali, J.E.M. Haverkort, E.P.A.M. Bakkers, Nanotechnology 23 (2012) 495305.

[296] X. Dai, A. Messanvi, H. Zhang, C. Durand, J. Eymery, C. Bougerol, F.H. Julien, M. Tchernycheva, Nano Lett. 15 (2015) 6958–6964.

[297] M. Chen, E. Nakai, K. Tomioka, T. Fukui, Appl. Phys. Express 8 (2015) 12301.

[298] R. Jafari Jam, M. Heurlin, V. Jain, A. Kvennefors, M. Graczyk, I. Maximov, M.T. Borgström, H. Pettersson, L. Samuelson, Nano Lett. 15 (2015) 134–138.

[299] M. Woodhouse, A. Goodrich, www.nrel.gov/docs/fy14osti/60126.pdf (2013) 1–50.

[300] M. Heurlin, M.H. Magnusson, D. Lindgren, M. Ek, L.R. Wallenberg, K. Deppert, L. Samuelson, Nature 492 (2012) 90–94.

[301] M. Bosi, C. Pelosi, Prog. Photovolt Res. Appl. 15 (2007) 51–68.

[302] F. Yang, M.E. Messing, K. Mergenthaler, M. Ghasemi, J. Johansson, L.R. Wallenberg, M.E. Pistol, K. Deppert, L. Samuelson, M.H. Magnusson, J. Cryst. Growth 414 (2015) 181–186.

[303] W. Metaferia, A.R. Persson, K. Mergenthaler, F. Yang, W. Zhang, A. Yartsev, R. Wallenberg, M.-E. Pistol, K. Deppert, L. Samuelson, M.H. Magnusson, Nano Lett. 16 (2016) 5701–5707.